UC San Diego
UC San Diego Previously Published Works

Title

Interplanetary scintillation (IPS) analyses during LOFAR campaign mode periods that include the first three Parker Solar Probe close passes of the Sun

Permalink

https://escholarship.org/uc/item/6k96d6fx

Journal

Advances in Space Research, 72(12)

ISSN

0273-1177

Authors

Jackson, BV
Tokumaru, M
Fallows, RA
et al.

Publication Date

2023-12-01

DOI

10.1016/j.asr.2022.06.029

Peer reviewed

eScholarship.org Powered by the California Digital Library
University of California

Available online at www.sciencedirect.com

ScienceDirect

Advances in Space Research 72 (2023) 5341–5360

ADVANCES IN SPACE RESEARCH (a COSPAR publication)

www.elsevier.com/locate/asr

Interplanetary scintillation (IPS) analyses during LOFAR campaign mode periods that include the first three Parker Solar Probe close passes of the Sun

B.V. Jackson [a,*], M. Tokumaru [b], R.A. Fallows [c], M.M. Bisi [d], K. Fujiki [b], I. Chashei [e] S. Tyul'bashev [e], O. Chang [d], D. Barnes [d], A. Buffington [a], L. Cota [a], M. Bracamontes [a]

[a] Center for Astrophysics and Space Sciences, University of California, San Diego, LaJolla, CA 92093-0424, USA
[b] Institute for Space-Earth Environmental Research, Nagoya University, Furo-cho, Chikusa-ku, Nagoya 464-8601, Japan
[c] ASTRON, The Netherlands Institute for Radio Astronomy, Oude Hoogeveensedijk 4, 7991 PD Dwingeloo, the Netherlands
[d] RAL Space, United Kingdom Research and Innovation – Science & Technology Facilities Council - Rutherford Appleton Laboratory, Harwell Campus, Oxfordshire OX11 0QX, United Kingdom
[e] Lebedev Physical Institute, Pushchino Radio Astronomy Observatory, Pushchino 142290, Russia

Received 7 March 2022; received in revised form 6 June 2022; accepted 11 June 2022
Available online 17 June 2022

Abstract

The University of California, San Diego (UCSD) time-dependent three-dimensional (3-D) reconstruction technique provides volumetric maps of density, velocity, and solar surface extrapolated magnetic fields by iteratively fitting our kinematic 3-D model to interplanetary scintillation (IPS) observations. While we currently use data from the Institute for Space-Earth Environmental Research (ISEE), Japan, we have also integrated this system adding data from Worldwide IPS Stations (WIPSS) network groups to increase both spatial and temporal coverage when these data are available. Some of these stations, especially the LOw Frequency ARray (LOFAR), centered in the Netherlands, currently operate in "campaign" mode only during periods of interest when the Parker Solar Probe (PSP) makes close passes to the Sun. The UCSD 3-D iterative reconstruction technique is unique in its ability to yield a low-resolution seamless extension of density and velocity parameters measured in situ, going outward into the surrounding interplanetary medium at the resolution of the volumetric data. We here present analyses using archival data sets from both ISEE, LOFAR, and BSA3 (Pushchino, Russia), mostly during PSP close passes of the Sun. These analyses provide the location of all inner planets from Mercury to Mars, and the spacecraft PSP, BepiColombo, and Solar Orbiter in the 3-D reconstructed volumes and can show the heliospheric structures that reach them as in-situ predictions of the structures present and forecasts of these parameters in near real time compared with near-Earth data sets.
© 2022 COSPAR. Published by Elsevier B.V. This is an open access article under the CC BY license (http://creativecommons.org/licenses/by/4.0/).

Keywords: Interplanetary Scintillation (IPS); Heliospheric physics; Space weather forecasting

1. Introduction

The solar wind is a hot, strongly turbulent, and high-speed expanding plasma of the solar atmosphere. The bulk of the plasma accelerates up to speeds of about 400 km s^{-1}. On average, individual features in the ambient solar wind traverse the ~1 AU distance between Sun and the Earth's magnetosphere in about four days. Structures such as coronal mass ejections (CMEs) and especially their interplanetary counterparts (ICMEs) are thousands of times larger than Earth at 1 AU, and often travel faster than the

* Corresponding author.
E-mail address: bvjackson@ucsd.edu (B.V. Jackson).

https://doi.org/10.1016/j.asr.2022.06.029
0273-1177/© 2022 COSPAR. Published by Elsevier B.V.
This is an open access article under the CC BY license (http://creativecommons.org/licenses/by/4.0/).

background solar wind; the very fastest reach Earth in less than a day. These transients can strongly perturb the near-Earth geomagnetic field through magnetic reconnection and by the exchange of energy from the solar wind. Accurate simulation of the evolving, background solar wind is crucial for predicting the structure and parameters of stream interaction regions (SIRs), and CMEs propagating through and interacting with background solar wind structures.

Since early in this century the University of California, San Diego (UCSD) has provided unique modeling to predict heliospheric density and velocity parameters in the inner heliosphere in three dimensions (3-D) and forecast CME arrivals. This iterative time-dependent tomography analysis uses interplanetary scintillation (IPS) data (Clarke, 1964; Hewish et al., 1964; Houminer, 1971) for depicting heliospheric structure. When more than one radio array separated by 100 km to $\gtrsim$ 1000 km views the same radio source at the same time, the cross correlation of the variable pattern signal gives a robust value of speed that can be transferred outward to provide the distribution of solar wind speeds perpendicular to the line of sight (LoS) (Fig. 1). The scintillation level from either array gives a proxy for bulk density (see Tiburzi et al., 2022). Our modeling employs IPS data from the Institute for Space-Earth Environmental Research (ISEE, formerly the Solar-Terrestrial Environment Laboratory, STELab), Nagoya University, Japan (Tokumaru et al., 2011) available in near real time at: https://stsw1.isee.nagoya-u.ac.jp/pub/vlist/rt/.

Early versions of the UCSD 3-D reconstruction assumed that the heliosphere corotates with the Sun (Jackson et al., 1998). Corotating 3-D reconstruction only allows solar rotation to provide perspective views. We later included changes in the outward–moving structure to also provide this perspective (Jackson et al., 2001, 2003). This allows both the motion of structures that are tracked as they move outward, and their outward-changing LoS weight to provide global time-varying 3-D reconstructions.

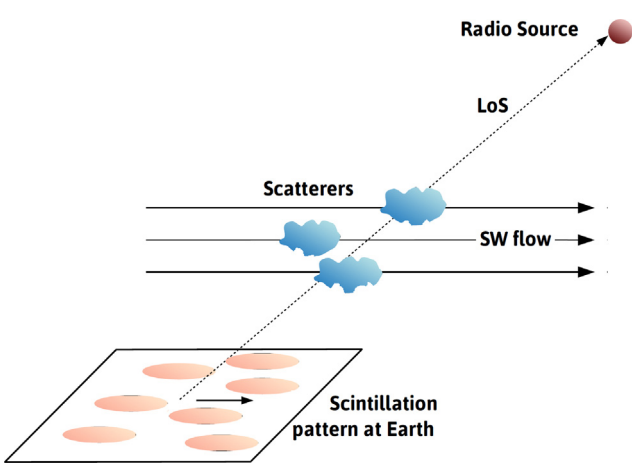

Fig. 1. IPS scatterers along a LoS to a point-like radio source produce an intensity pattern on the surface of the Earth moving outward from the Sun at solar wind speeds.

The appropriate line-of-sight (LoS) weighting for these structures is derived from theoretical weak scattering theory (Young, 1971; Kojima et al., 1998). Descriptions of how this works to differentiate different structures is described more fully in Jackson et al., (2020). The number of volume elements that can be determined in this way is generally about the same as the numbers of lines of sight (LoS), and thus with only a few thousand scintillation level LoS in a given Carrington rotation, and a few hundred of velocity, there would be too few samples to make complete 3-D reconstructions of the structures present if we were unable to iteratively fit the LoS values that exist to a solar wind model. The UCSD 3-D reconstructions used with much success to date (Jackson et al., 1998) have been provided by a kinematic model that conserves mass and mass flux and assumes radial transport from the Sun as structures move outward.

To iteratively fit a solar wind model, the LoS segment 3-D weightings are projected back in space and time using a programming algorithm we term a "traceback matrix" to a solar wind inner boundary "source surface" that is usually set at 15 solar radii (Rs). The traceback matrix gives the origin location and time of each solar wind volume element on the source surface. This matrix also provides the differences (in density, and velocity) of the material in the volume element from those of its origin. At the inner boundary the changes from each LoS are combined and smoothed, and with their individual weights formally inverted to give new boundary conditions for the next solar wind model. Only the source surface locations that provide more than one LoS crossing can be inverted and yet each model LoS must be filled to give a proper comparison with an observation from the same location. Thus, each boundary on each source surface is filled completely by a system of Gaussian spatial and temporal filters in locations that cannot be inverted. Extensive study of this process has shown that the final iterated values are insensitive to starting source surface values, and that most of the convergence occurs within one or two iterations (Jackson et al., 1998, 2008a, b). Often the locations within the model that are not reached by the inversion process, are left unfilled in the final volumetric result.

These 3-D reconstruction analyses provide a global 3-D prediction of heliospheric structure in the plasma parameters, velocity, density, and magnetic field without making assumptions about their morphology, such as size, continuity, and shape as a loop, bubble, or curved or elongated structure. The only assumption made is that the structure fits the observations smoothly at the permitted spatial and temporal resolutions, and that mass and mass flux is conserved for the material that is transported radially outward from the Sun. The IPS data contains information about both solar interaction regions (SIRs) that usually have a base in the corona as streamers, and fast transient events such as CMEs. Many of the structures mapped here have been characterized by others (e.g. see Viall et al., 2021, and references therin) as background solar wind, CMEs,

SIRs, or corotating structures (having emanated from the same location on the Sun for at least one 27-day solar rotation as observed at Earth). These are all observed in the IPS 3-D reconstructions and some of these, such as large CMEs are obvious. However, CMEs often linger and remnants rotate with the Sun for more time than they are observed in coronagraph views, and corotating structures blend with the background solar wind and can be highly variable such that they are often difficult to distinguish from CMEs by their morphology alone. For this reason in most analyses where we fit these data sets in low resolution, we usually do not distinguish between the different heliospheric structures observed unless it is to help forecast their arrival at Earth. Many good examples of these 3-D reconstructions in conjunction with CMEs are found in the literature, including two articles in this issue by Fallows et al. (2022), and Iwai et al. (2022). Here the details of both a CME (or set of CMEs) and the surrounding structures have been studied in detail, and also 3-D reconstructed using the ISEE IPS analyses.

IPS groups at Nagoya University, Japan, Pushchino, Russia, using the Big Scanning Array version 3 (BSA3), and at the Geophysics Institute, UNAM, who operate the MEXART array in Michoacán, Mexico (Gonzalez-Esparza et al., 2017), currently have radio systems that regularly provide IPS data for their own use. The Rutherford Appleton Laboratory (RAL Space), UK; the Ooty radio array in India (Manoharan, 2010); and the groups with BSA3, and MEXART data have used the UCSD time-dependent program in processing archival data sets. The ability to provide data in near real time adds more complexity to IPS data taking, mostly in the way that the IPS data needs to be processed, edited, and presented for use over the internet, and so far only the data from ISEE, Japan has been made available in this way. Thus, so far, the UCSD near real time analysis only incorporates the IPS data from ISEE, Japan. Currently this modeling technique now operates at UCSD, the NASA Goddard Community Coordinated Modeling Center (CCMC, Maryland), George Mason University (GMU, Virginia), the Korean Space Weather Center (KSWC), and at the UK Met Office.

The IPS observations, as explained prior, are a sparse data set that are used to fit a solar wind model. The greater the number of LoS that are available to provide data, generally the better the fits in the 3-D reconstruction perspective views. In addition fits to IPS sources in the sky near the Sun from a single site can only do this for half of the day; for meridian transit instruments like those in ISEE, Japan, there is only one view of any given source possible each day. Very fast transient events (Coronal Mass Ejections - CMEs) have been known to cross the distance from the Sun in less than one day, and thus the fastest CMEs can be missed by a radio array system situated at a single Earth longitude. The ISEE radio array has been lucky to observe both the Bastille Day CME (July 14, 2000) and the Halloween Storm Event (October 28, 2003) adequately enough to view them and map their structures in transit from the Sun (Jackson et al., 2003, 2011a; Tokumaru et al., 2003, 2007) for a review of these events see Cliver and Dietrich, 2013). For the Carrington event of July 23, 2012 (see Baker et al., 2013; Russell et al., 2013), that erupted from the Sun to the west and was seen moving outward at 3:40 UT in coronagraph images, narrowly missing Earth, the ISEE system was not as lucky. The Sun transits at about 3 UT in Japan, and by the next day at 22 UT when the ISEE array was able to view radio sources to the west of the Sun, the CME had nearly passed the field of view covered by this single radio system.

This known vulnerability of the IPS analyses to the fastest and most damaging CME events has provided one incentive for the idea of a Worldwide Interplanetary Scintillation Stations (WIPSS) network concept (Bisi et al., 2016, 2017). Earlier, at the Third Remote Sensing Workshop held 20–24 October 2015 in Morelia, Michoacan, Mexico 2015; 1) a standardized IPS format was settled upon; and 2) all participants agreed to share their data, host the requisite websites for this sharing, and display their data sets in near real time. First to provide IPS data in the standard format was the group from ISEE Japan, followed shortly by those working on the Low Frequency Array (LOFAR, van Haarlem et al., 2013) data at the Rutherford Appleton Laboratory, UK, and based in ASTRON, the Netherlands. Others including those at the MEXICO (SCiESMEX) array (Gonzalez-Esparza et al., 2017), have promised data from their system. The other recent member joining the group has provided access to a portion of their data from the world's largest (70,000 m^2) currently operating radio array; the 111 MHz system at Pushchino, Russia. The Chinese, too, have joined in with an effort underway to provide a dedicated IPS system (with a main station at Ming'antu, Inner Mongolia). Over the last years since 2015, UCSD has modified its tomography program to use a new standardized IPS format, and provide simultaneous inputs from as many radio observatories as are able to share their data via internet access either for archival analyses or in near real time for forecasting purposes.

Prior to the Parker Solar Probe (PSP) launch on 12 August 2018, a LOFAR campaign in September 2016 was organized to provide IPS inputs from extant WIPSS members. The intent was to get ready to continue IPS data taking and research at these individual institutions, and add data to the UCSD IPS tomography where this was possible. Most of these groups have persisted in their data-taking. The most successful of these various IPS efforts to date has come from an amalgamation of ISEE data with that from the LOFAR array during periods when LOFAR was able to be operated in campaign mode centered on the PSP close passes to the Sun. The following analysis is intended to show how each IPS system can be used and blended to give consistent results globally. It is not intended to show how well these calibrate with PSP in-situ measurements which is the subject of a different

article requiring more PSP IPS data than is currently available from other than ISEE. During the first three PSP close pass periods LOFAR has been able to view as many different radio sources as ISEE to provide multi-site LoS velocities and most recently *g*-level values of scintillation strength. In Section 2 we describe the methods used to provide these data sets in the standard format. In Section 3 we present our results, and give examples of the benefits in providing them from different solar locations. In Section 4, we discuss some of the ideas put forward about how we can provide better results from the WIPSS effort and current knowledge of the in-situ measurements from PSP when many different systems work together. We conclude in Section 5. We follow the conclusions and references with two appendices that explain a standard format now used in listing IPS radio source analyses, and a table that lists specifics of the amounts of data used from each radio site in this article.

2. IPS data analysis and the standard format

IPS data have been analyzed in many different ways over the years and here we describe the technique settled upon by the Japanese to map both scintillation level and to also provide a robust velocity from multiple radio arrays. These data are currently utilized by UCSD in its 3-D time-dependent reconstruction technique both in near real time analyses operated at UCSD and at other sites and for scientific studies using archival data sets. There is essentially no difference in the two analysis types except that with archival data sets it is possible to use the IPS and in-situ data following the time of interest. This provides the most complete reckoning of heliospheric structures that pass in-situ locations to an outer boundary where the signal to noise along a LoS no longer gives a meaningful measurement. This LoS distance is usually set at 3 AU which means that the reconstructed data benefits from IPS data obtained for up to ~12 days following the run time of the analyses. By this time all structures that were earlier observed near the Sun have passed this distance in the inner heliosphere. For forecast analyses only data obtained before the run time can be used to provide the analysis.

The scintillation strength of a point-like radio source is generally determined by a Fourier transform of the scintillating source time series over a period of ~10 s duration. This allows presentation of the scintillation power of the source shown in blue in Fig. 2. At the ISEE radio frequency of 327 MHz the spectral frequency value f_L is usually set at ~0.1 Hz and f_{max} at ~25 Hz. At ISEE the scintillation power is determined between these values of f_L and f_N. The value of f_N varies depending on the IPS observations, and at ISEE f_N, a corner frequency between the IPS power and noise spectrum is determined for each observation. At the ISEE 327 MHz radio frequency the heliospheric scintillation power maximizes at a spectral frequency of about 1 Hz, but at lower frequency can be contaminated by ionospheric scintillation, and thus the value

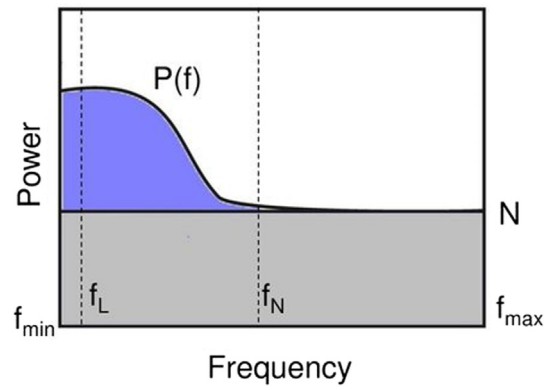

Fig. 2. The power spectrum of a scintillating source is shown in blue above the source non-scintillating power shown in grey.

of f_L needs to be at a spectral frequency value where there is enough power measured in the spectrum, and yet little or no ionospheric scintillation present. This can only be determined by individual spectral measurements for radio sources at different radio sites and at different times since the amount of ionospheric scintillation is dependent on the site Earth latitude, and whether or not a geomagnetic storm is in progress. As long as f_L is kept the same throughout the source observation over the year and as far from the location where the scintillation power decreases rapidly for the specific radio site, the exact value of this frequency becomes relatively unimportant in the calculation of the relative value of scintillation level, *g,* over time in the equations shown below. If the background source value *N* is known, as in Fig. 2 it can be used to normalize the source power after its subtraction by dividing by this value to give the scintillation level as in Eq. (1):

$$\Delta S = \sqrt{\int_{f_L}^{f_N} (P(f) - N) df / N} \tag{1}$$

where *P(f)* is scintillation power from the time series as shown in Fig. 2 integrated over the time series frequency range shown. Usually over the few minutes a source is observed, the different 10 s scintillation powers determined can be added to give a daily source standard mean value, and an error estimate. Fig. 3 shows log–log plot of ISEE IPS data, scintillation levels for the radio source 3C273 over the period in the year the source could be observed. This type analysis is provided for each ISEE source observed to give a least squares fit slope values as in Eq. (2) (Tokumaru et al., 2000):

$$\Delta \bar{S}(R) = aR^{-b} \tag{2}$$

where *a* and *b* are respectively a constant and a power used to fit each radio source as shown in Fig. 3. These values are determined for the yearly source values in weak scattering which at 327 MHz radio frequencies begins at a LoS close distance to the Sun (P-Point distance) of about 0.2 AU (~41 Rs or an elongation, Є = 11.5°) and continues out-

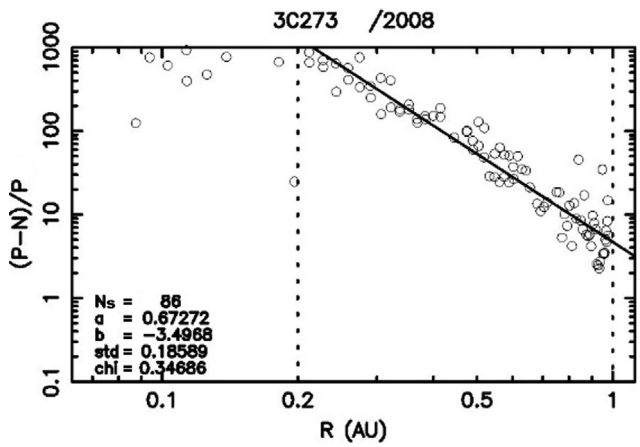

Fig. 3. Plot of normalized source power vs LoS distance for radio source 3C273 during 2008. For this plot the number, Ns, of radio source observations, a and b of equation Eq. (2), the standard deviation (std) of source values relative to the linear fit, and the goodness of the fit relative to the expected value at the line (chi) are given to the lower left.

ward in elongation until the scintillation level becomes too low relative to the background noise level to provide reliable results. Locations for weak scattering depend on the radio frequency and begin at LOFAR or Pushchino data at 150 MHz or 111 MHz, the weak scattering regime extends beyond elongations of 20° (0.34 AU) and 21° (0.36 AU), respectively. The yearly source values for Eq. (2) are first fit by all source values R > 0.2 AU; then ΔS values with deviations $> \pm 2\sigma$ are discarded and the function is fit again. The 2008 yearly fit to the sample source 3C273 shown in Fig. 3 has values of the number of daily source observations Ns, a, and b given on the figure with a standard deviation from a straight line of ~0.19. In Fig. 3 there were 86 days where a valid source value could be used. The radio source 3C273 is a strong point-like radio source, and frequently for other radio sources there are not as many source values that can be used to provide a g-level value. In using ISEE data we require that at least eight days of valid source values are necessary to determine a g-level. Similar minimum numbers of source values are required to determine g-levels at the other radio sites.

For all three radio sites described here, a calculation of the power spectrum was provided as in Fig. 2 for each radio source that was observed. Although the analysis over the period of the source observation for a given year was used to provide a log–log plot as in Fig. 3 with solar distance for ISEE data, slightly different ways were used to provide a g-value for Pushchino and LOFAR data. For the short times available from the Pushchino data, a simple straight line log m linear in time fit covering about two weeks of data was all that could be used. Similar ISEE comparisons, with Pushchino data for a different time period than studied here, are discussed more thoroughly in Tokumaru et al. (2019). For LOFAR data, which were also of shorter duration over time, a source elongation linear fit was substituted for time. As long as values of the source trend can be determined with low-enough values of certainty over solar distance, this type of technique will work for any radio frequency. As a final note, the observation time for a radio source to be fit is usually limited to one year or less since it is known that some sources can vary slowly in scintillation strength over periods of years either intrinsically, or from intervening interstellar material.

Once an average slope is determined, an IPS g-level value that gives a standard variation of scintillation level for each source is made as in Eq. (3):

$$g = \frac{\Delta S}{\Delta S(R)} \tag{3}$$

where values of ΔS are the ISEE daily source scintillation level values divided by the mean value for that period over many days as in Gapper et al. (1982). UCSD has then used these to determine a model value from interplanetary density as in Eq. (4):

$$g = AR^{\alpha}Np^{\beta}, \tag{4}$$

where A is a constant, R is the radial distance from the Sun raised to the power α, Np is the proton bulk density raised to the power β. The constant A and values of the powers α and β have been determined from past analyses using the UCSD 3-D reconstruction technique and iterative fits to bulk proton density at Earth as described more and referenced as above in Tiburzi et al. (this issue), or Jackson et al. (2020). With in-situ values from PSP the values of α and β have a more exact way of being refined since both vary with distance from the Sun; α most directly and β through the value of Np. However, both density and velocity parameters can vary beyond the assumptions of mass and mass flux conservation and these two parameters need to be provided as average values over time. The parameters α and β were determined thoroughly at the beginning use of the IPS tomography analysis (Jackson et al., 2003) by fitting the ISEE time series densities and velocities over Carrington rotation intervals for a large CME that arrived at Earth providing a significant enhancement of density and a large change in velocity. This was done by varying these two parameters simultaneously to provide the best Pearson's "R" correlations and one-to-one fits similar to those shown in this article in the figures of Section 3. The constant A is used to weight each total LoS contribution the same, and the values of α and β, were chosen as 3.60 and 0.70, respectively, by comparing them with Advanced Composition Explorer (ACE) (Stone et al., 1998) Solar Wind Electron Proton Alpha Monitor (SWEPAM) (McComas et al., 1998) level zero data for different Carrington rotation intervals. These parameters have been checked with other Carrington intervals over time, and compared with other near-Earth spacecraft data, but have remained the same since first determined. We have also checked these parameters using the analysis at different radio frequencies, but have so far found no consistent trend requiring a change in the existing values. The parameters α and β are able to be set when the tomography program is run, and we intend

that these be checked regularly. The value of α has the least effect near Earth in providing changes to the density at that location. The parameter β has the most effect in modifying the tomography IPS bulk density value to fit in-situ measurements. We note, however, that even at the low temporal resolutions that can be reconstructed by the IPS analyses, the variation in measured amplitudes from different near-Earth in-situ monitors can differ by a factor of two for the same heliospheric structure. In all comparison analyses one-hour average data are used from the different monitors, and then boxcar averaged to a one day cadence to fit the low resolution results predicated by the tomographic Gaussian filters that smooth the 3-D reconstructed analyses.

Robust IPS velocities for the solar wind can be gotten by cross-correlating the IPS signal from one LoS to another for a given radio source. This provides an offset for the mean of the outflowing scintillation patterns along the LoS. A sample cross correlation pattern for two radio sites is shown in Fig. 4 (and see Fallows et al., 2022 for further examples). Only two LoS to a source are required to provide a speed when the outflow is assumed radial from the Sun on the projection plane shown in Fig. 1 (Earth). However, an error relative to the radial can be obtained when three or more observations of the same source are obtained over the same time period. At large site distances between LoS views, the scintillation pattern lag values generally provide lower cross correlation amplitudes than when sites are closely spaced. When sites are distant from one another the cross correlations can show more than one single velocity peak, attesting to the different dominant LoS heliospheric structure speeds measured over the same time period (*e.g.*, Breen et al., 1997). In the UCSD 3-D reconstruction program using ISEE data the cross correlation offset peak is interpreted as an ensemble speed of the solar wind plasma perpendicular to the LoS from the Sun and fit by the integrated LoS model speed.

The standard format developed for use by the Worldwide IPS Stations (WIPSS) network group provides a way to express speeds and *g*-level values of IPS sources in a consistent way. These observations are presented in an ASCII format, one line per radio source with values separated by spaces. These values include the observation time of the radio source, the duration of the observation in minutes, the site providing the analysis, the source name, the source J2000 coordinates, its elongation at the time of observation, IPS speed, and *g*-level value, and the observational errors for these two latter quantities. There is more than one way to provide speeds and *g*-level values, especially when multi-site or single-site measurements are determined, and thus the observational values are repeated with the way the observation is made indicated following their values. A full listing describing the standard format is given in Appendix 1 at the end of this article. The numbers of radio sources used generally determines the quality of the tomographic 3-D reconstructions, and these values for each of the Carrington rotation intervals studied below are given in Table 2 in Appendix 2.

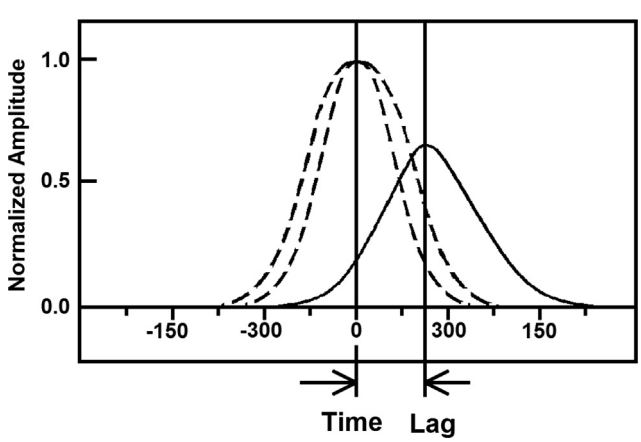

Fig. 4. IPS pattern autocorrelation for both observed radio sources and a cross correlation for a sample radio source. Here the time lag is associated with a pattern speed in kms^{-1} along the solar radial direction.

3. Results from the data set combinations

3.1. 2016 Campaign ISEE-LOFAR-Pushchino

Combining data for the different stations worldwide gives analyses that are improved over those when one site alone is used. The first of these periods shown describes the results from a time interval in September to November 2016 when archival data from ISEE, LOFAR, and Pushchino IPS observatories were analyzed and combined in the UCSD 3-D reconstruction analyses. At this time ISEE IPS data from both velocity and *g*-level were available, only IPS velocity from LOFAR was available, and only *g*-level data was available from Pushchino. The LoS weighting for the different frequencies used is not exactly the same. Fig. 5 shows the LoS weighting or wavelength dependence of the modulation for different thickness layers

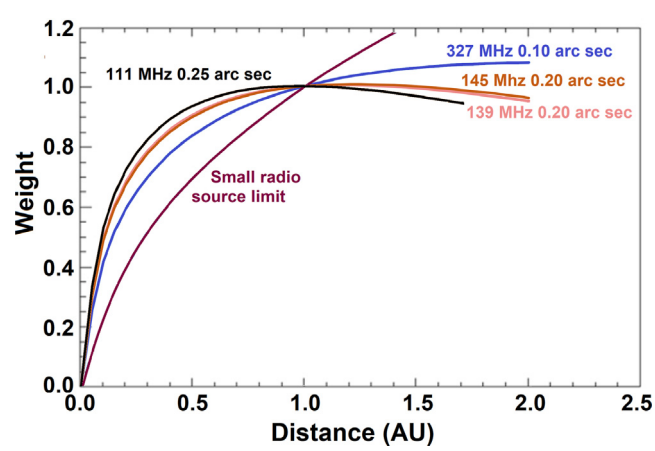

Fig. 5. LoS weighting normalized to 1 AU used in the 3-D reconstruction tomography at ISEE (327 MHz), LOFAR (139 and 145 MHz), and Pushchino (111 MHz) assuming source sizes for the scintillators of 0.10, 0.20, and 0.25, arc sec respectively. A bound for radio sources of minimum size is also shown.

for the three different radio sites and frequencies as specified for weak scattering by Young (1971) assuming a homogenous interplanetary medium of electron density scatterers. Although the different weighting curves have similar shapes, the weighting values vary with radio frequency and the source size for each LoS. The minimum source size provides a weighting as given in Fig. 5. A larger source size provides less total scintillation but heavily weights the portion of the LoS close to the Earth. Following this, the weighting is modified significantly by the specific solar distances and scattering densities assumed present along the LoS in Eq. (4). While older sites are tuned to provide IPS data near a single frequency, the frequency-agile LOFAR array is unique in its ability to record different radio frequencies, and has provided IPS data at frequencies of from 139 MHz to 146 MHz for the years 2016 – 2019 for these analyses. Each weight is used along with the values of bulk density and the parameters of Eq. (1) to provide the model weights for each observed radio source. Fig. 6a & 6b shows a sample fisheye skymap of the combined velocity analyses from LOFAR and ISEE IPS data when all three IPS data sets were used in the combined 3-D reconstructions. In these skymap presentations, elongation angle is linear from the Sun in the center of the plot to the outer edge of the plot with 45° and 90° elongation, the ecliptic (horizontal), and the meridian through Earth marked on the image. The fit of the IPS source velocities perpendicular to the LoS within 3 h of the model values are shown here superimposed onto the model values. Fig. 6a and b are presented in velocity perpendicular to the LoS and the superimposed source color coded with its observed velocity value (see scale to the left). The source is compared with the LoS value of the model, in this case an instantaneous model determined at the time indicated at the source LoS location (within 3 h of the measurement). If the source value is enclosed by a white circle, the observed value is less than

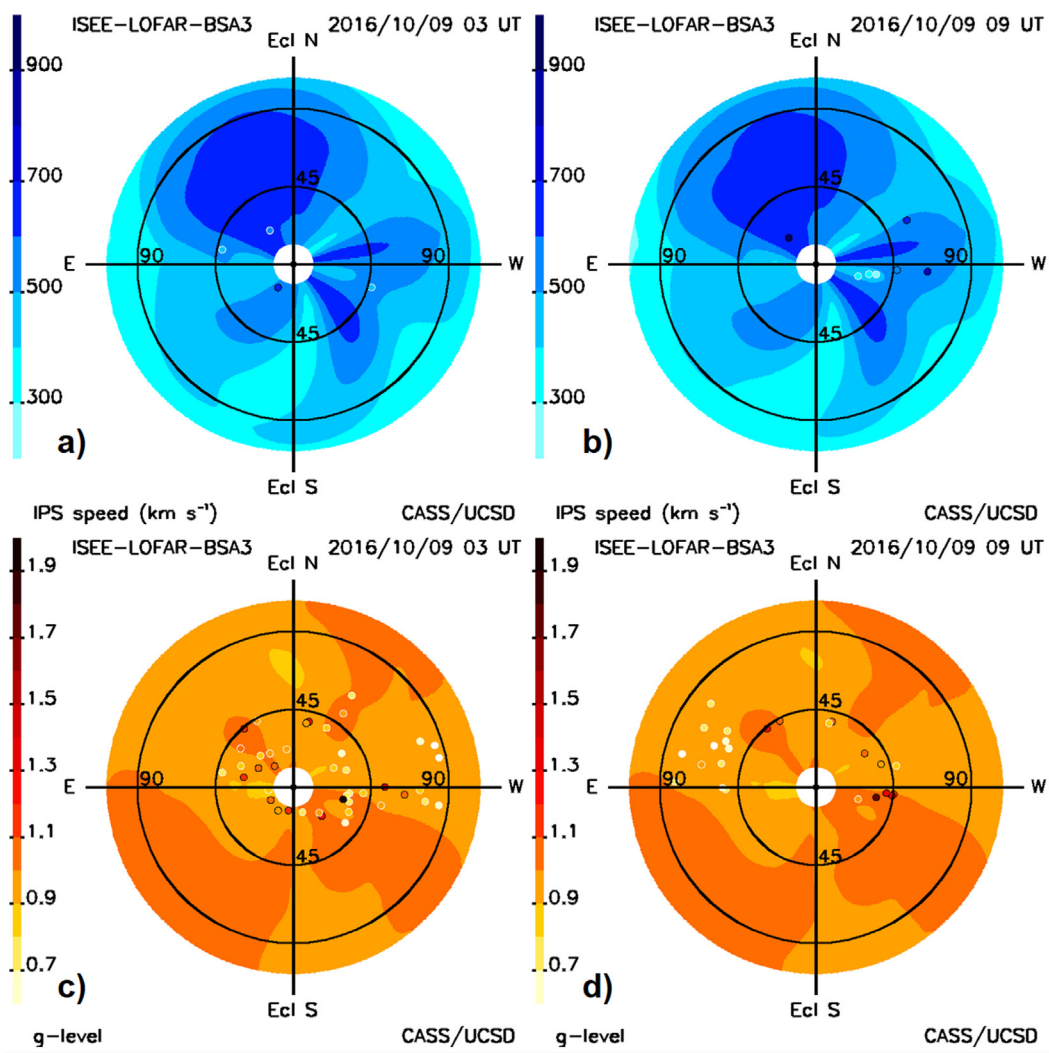

Fig. 6. Modeled IPS perpendicular velocity values fit to the radio source LoS observed values (locations are shown by circles) shown as fisheye skymaps **a)** from ISEE **b)** from LOFAR. IPS *g*-level values fit to the radio source LoS observed values (locations are shown by circles) **c)** from mostly ISEE data east and within 45°, and to the west > 45° data and in **d)** to the west *g*-level data are from Pushchino.

the model. If enclosed by a black circle the source has a greater value than the model. Fig. 6c & d shows similar fisheye skymaps of the observed *g*-level values fit to the modeled *g*-level values within ± 3-hours of the time shown on the image. In these maps elongation is plotted on a linear scale. Note that in Fig. 6 although the times when the majority of sources are observed near the Sun are not the same, often the same radio sources (that are known to be strong scintillators) are used in the observations from the different radio sites.

Over the period of 6 h from one to the other skymap, outward motion of the modeled heliospheric structures can be discerned. These sources and all others for a period plus or minus about five days provide the structures that are presented in the skymaps, since on average it takes about 10 days for the solar wind to travel outward from where the structures are first observed near the Sun until they reach the 3 AU limit of the volume that is reconstrupcted in 3-D. These radio sources all fit together to provide accurate in-situ values at Earth for the Carrington rotation interval reconstructed, as shown for the derived velocities and densities in Fig. 7. These analyses are compared with in-situ measurements from the SOlar and Heliospheric Observatory (SOHO) spacecraft (Domingo et al., 1995) Charge, Element, Isotope Analysis System (CELIAS) Proton Monitor (Hovestadt et al., 1995). Here we compare our analyses from only this near-Earth spacecraft, since at the time no data from the ACE spacecraft, or Wind spacecraft Solar Wind Experiment (SWE) (Ogilvie and Desch, 1997) were available. At the time shown, a small CME was headed toward Earth and its manifestation in the solar wind can be observed in a cut through the ecliptic for both velocity and density as shown in Fig. 8. To show heliospheric structure in approximately the same way from near the Sun to the largest distance from the Sun observed, density has had an r^{-2} fall-off removed and has been normalized to 1 AU. The small CME has a maximum density of about 6 particles cm^{-3} at Earth at about 03 UT on October 10. The fits here have been normalized by velocity and density as described by Jackson et al. (2010, 2013) to fit the IPS values by adjusting the g-level value of 1.0 to fit the mean of the density excursions throughout the Carrington interval 3-D reconstructed, and also by imposing a weighted tomographic fit with all

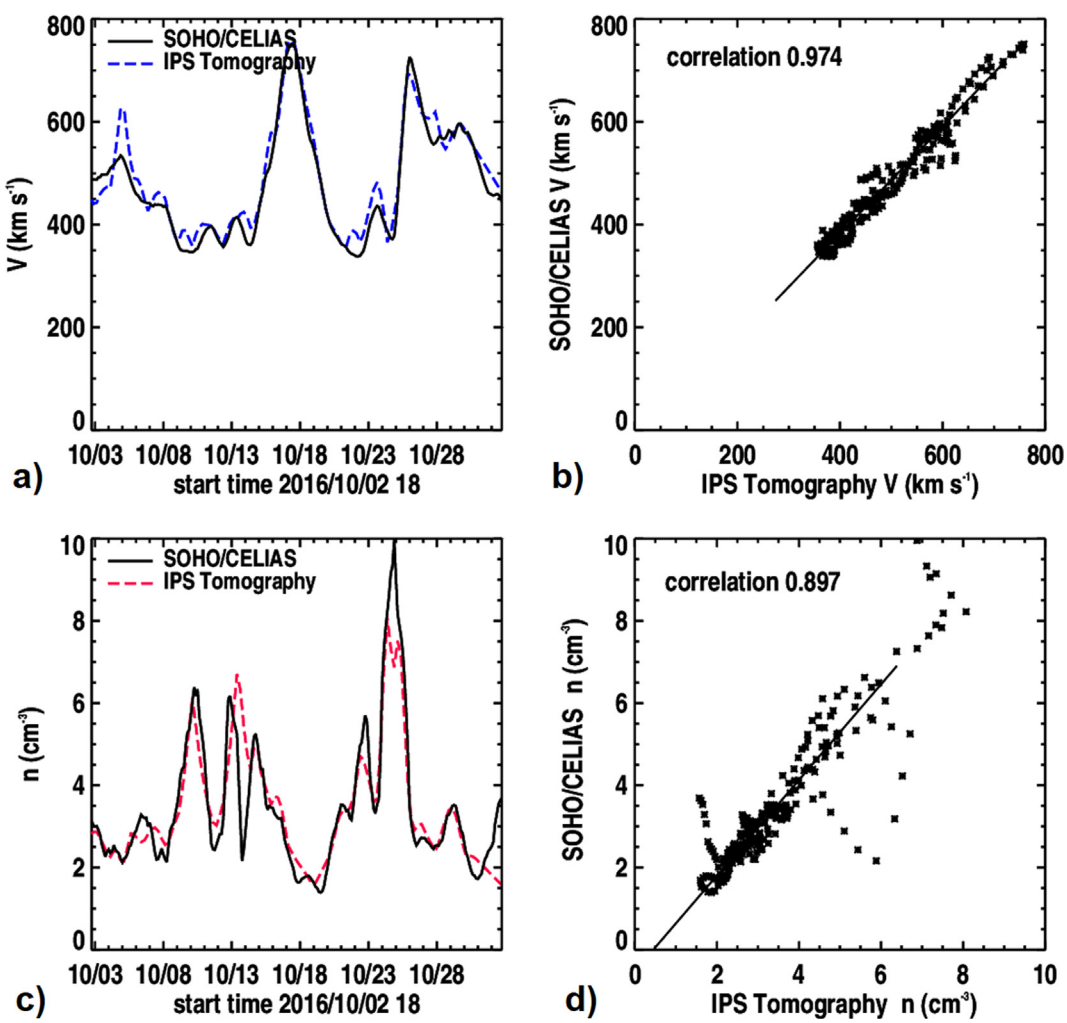

Fig. 7. **a)** IPS-derived velocities compared with CELIAS measured in-situ velocities. **b)** A Pearson's "R" correlation shows an approximate one-two-one fit and correlation value of 0.97. **c)** & **d)** IPS-derived densities compared with CELIAS measured in-situ densities with a correlation of 0.90.

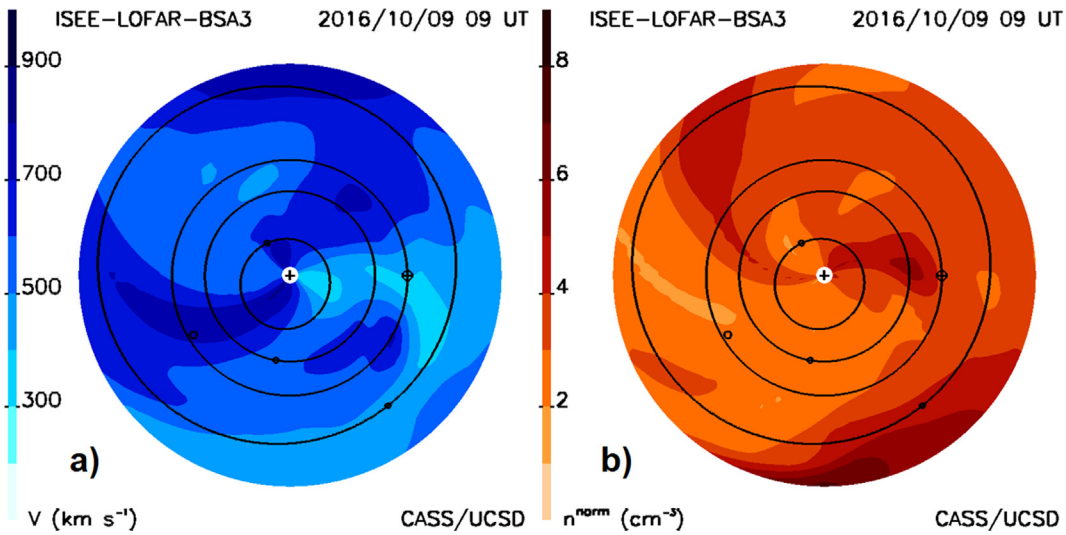

Fig. 8. Cut through the ecliptic plane of **a)** velocity and **b)** density at 09 UT on October 9, 2016. Earth is shown on its orbit to the right. The inner planets from Mercury to Mars along with their orbits, are also shown projected onto the ecliptic. The STEREO A spacecraft is shown as a small circle just inside Earth's orbit to the lower left.

others to each near-Earth LoS segment to the in-situ velocity or density measurements at Earth.

3.2. First PSP close pass LOFAR-ISEE

The first Parker Solar Probe close pass of the Sun occurred at 03:27 UT November 6, 2018 off the solar west limb seen from Earth at a distance of 0.17 AU. At the time of the PSP close pass, a small velocity increase was present at Earth (Fig. 9) following a density enhancement that was at maximum one day earlier. These values are registered in the ecliptic and meridional velocity and density cuts as shown in Fig. 10 on 03 UT November 4, 2018. Fig. 10 also includes velocity density meridional cuts through the PSP spacecraft at the same time (2 days before the PSP close pass of the Sun). Over this period, the PSP spacecraft from 11/1 through 11/5, retains the same heliographic longitude to within 5° of the center heliographic longitude of 319.3°, and varies from about 0.24 to 0.17 AU from the Sun. Thus, structures passing PSP in situ for about five days are primarily those that emanate from a single solar longitude. This same configuration occurs on the first three PSP passes, that all have perihelion distances of 0.17 AU. Although the IPS time-dependent analysis should show similar plasma features at these locations, this depends on the fidelity of the 3-D reconstructions in both latitude and longitude commensurate with the resolutions presently available from the IPS analyses which themselves have a resolution of about 10°. However, there is another large factor involved here, and this is a matter of background solar wind acceleration, which is not included in the current tomographic fitting analysis provided by Eq. (4). Our analyses to date conserve mass and mass flux without knowledge of the presence of this factor. We discuss this more fully and show an example of in-situ measurement comparisons of the PSP data with the 3-D reconstructions in Section 4.

3.3. Second PSP close pass LOFAR-ISEE

The second Parker Solar Probe close pass to the Sun occurred at 22:40 UT April 4, 2019 when PSP was 0.17 AU from the Sun. At mid-day April 8 both PSP and Earth were at the same heliographic longitude of ~11° (on the Sun-Earth radial) when PSP was 0.20 AU from the Sun, and ~3.4° above Earth in heliographic latitude. To provide the density analyses, IPS g-levels from ISEE are primarily the only values used. At this time, due to snow-loading on the mountain ISEE antennas, IPS velocities are primarily provided by LOFAR with only a very few present the very end of the period from ISEE. Because of this the velocity analysis from the LOFAR array is clearly very beneficial. The in-situ measurements near Earth are from ACE level zero data that was available throughout this period. Fig. 11 shows the coverage of the ISEE and LOFAR arrays on April 5, 2019, and times (6 h apart) when observations from both sites maximized as shown also for the 2016 data set in Fig. 6. As indicated, there is coverage from both instruments at this time with velocities for ISEE especially near the ecliptic. However, during this period and especially during the period following the PSP close pass both systems had outages for several days where little or no data were obtained. The heliospheric structures present observed at 09 UT April 8, 2019 are shown in Fig. 12, when PSP and Earth were on approximately the same ecliptic meridian. The PSP spacecraft corotates within 5° of the same heliographic longitude centered on 354.5° and 11.3°, respectively from 0.24 to 0.17 and 0.17 to 0.24 AU, at times 03/31 to 04/04 and 04/05 to 04/09. The velocities and densities of the encounters at Earth measured in situ

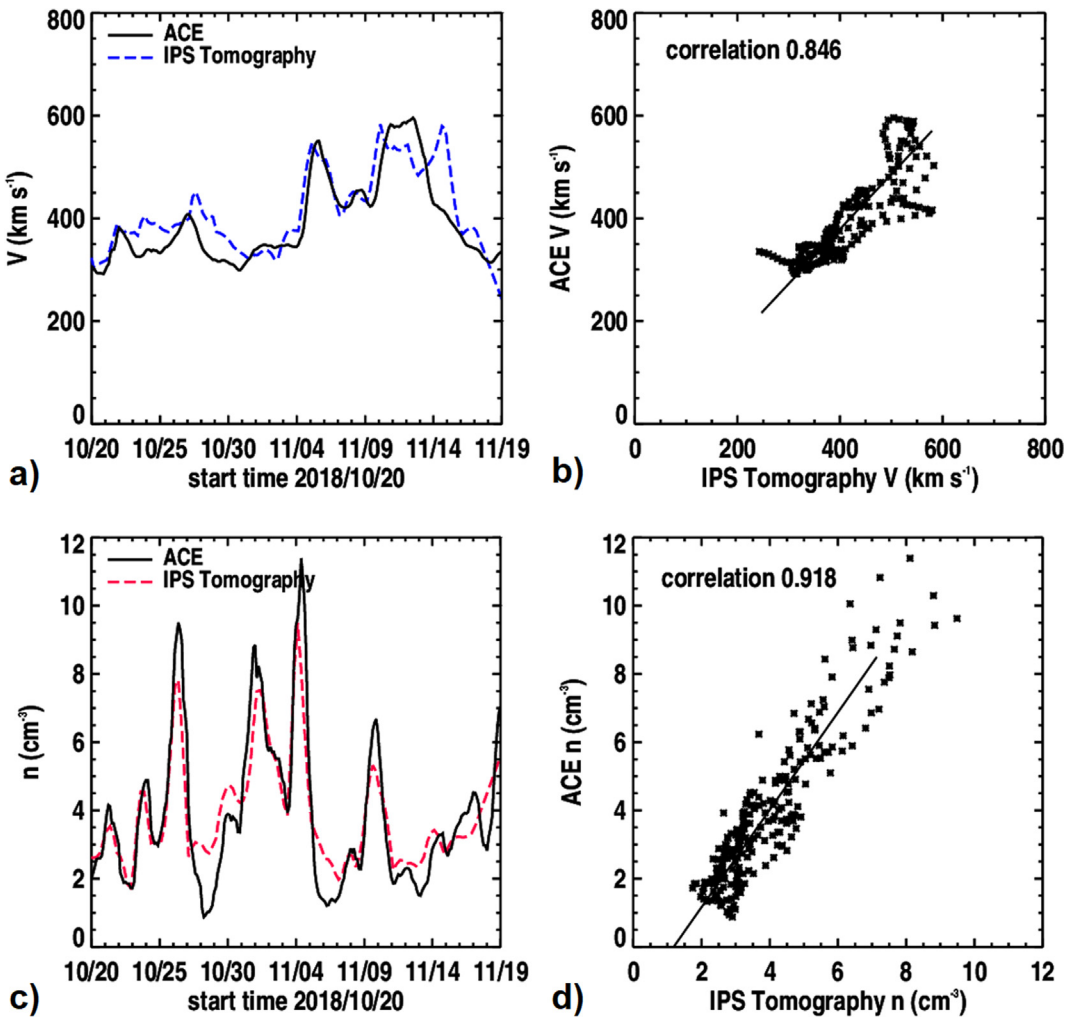

Fig. 9. **a)** IPS-derived velocities compared with measured ACE level zero in-situ velocities. **b)** A Pearson's "R" correlation shows an approximate one-two-one fit, and the correlation value of 0.85. **c)** & **d)** IPS-derived densities compared with measured ACE level zero in-situ densities have a correlation value of 0.92.

are shown in Fig. 13. Although the density changes fit well at Earth during this period, and the velocities also correlate fairly well with the NOAA provided in-situ measurements, there are few large changes in either velocity or density that dominate during this interval.

3.4. Third PSP close pass LOFAR-ISEE

The third Parker Solar Probe close pass of the Sun occurred at 17:50 UT September 1, 2019 when PSP again passed within 0.17 AU of the Sun. This time the PSP close pass occurred when much velocity and g-level data was available from both the ISEE arrays and LOFAR almost exactly when the PSP spacecraft was situated on the side of the Sun opposite Earth. Again as in the other periods studied, the near-Earth analyses and correlations are excellent for both velocities and densities; a large velocity increase observed from a corotating structure is well-observed in the middle of the period at Earth (Figs. 14 and 15). This has little to do with the structure observed at PSP because its close pass was on the side of the Sun opposite that from Earth, and thus is in a region where the 3-D reconstruction analysis can only be interpolated from radio source locations observed around the Sun's circumference beyond about 11.5° elongation.

4. Discussion

Here, and in the past, the main attempt has been to use the IPS analyses to provide good measurements of velocities, densities, and background magnetic fields at Earth with less consideration of the detail of the solar wind outward flow from the Sun. There is some evidence from magnetic fields observed at Earth that surface fields are delayed in outward flow from our extrapolation of them from the solar surface, generally by about a day (Jackson et al., 2019). We have assumed that CMEs, especially those that are fast, probably do not participate significantly in this delay. Now, however, there is significant velocity and density data from PSP, and so it become possible to use these

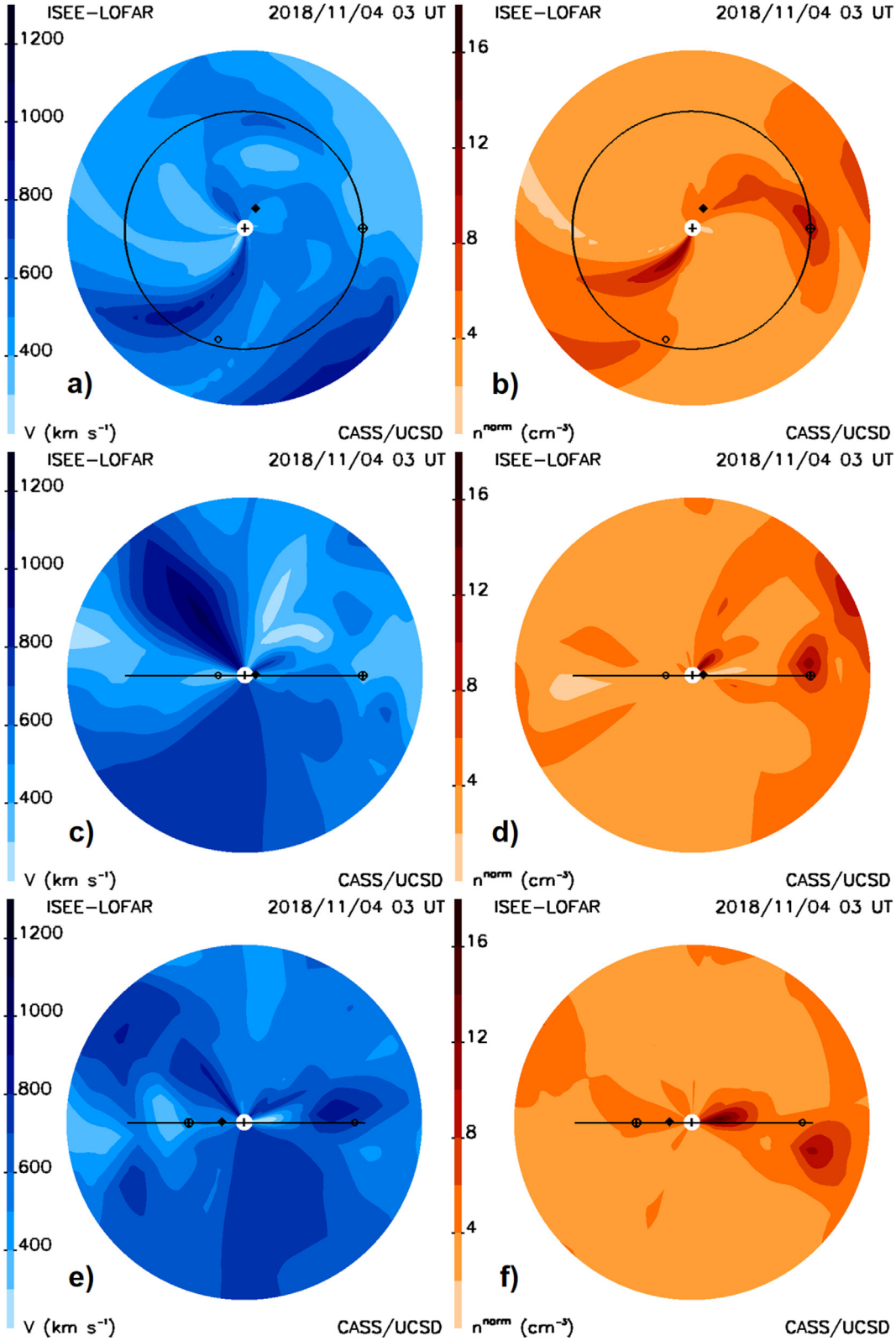

Fig. 10. **a) & b)** Cuts through the ecliptic plane of velocity and density at 03 UT on November 4, 2018. **c) & d)** Earth velocity and density ecliptic meridional cuts through Earth. **e) & f)** Velocity and density ecliptic cuts through PSP as viewed from a position opposite the Sun looking back toward the Earth. PSP is shown as a diamond with the Earth "⊕" projected on this meridional plane slightly farther outward from the position of the Sun than PSP.

analyses, and the assumption of mass flux conservation to determine the speed delay from PSP to 1 AU distances. One caveat we have found to this is that spacecraft at Earth can give a different result for density amplitude, of up to a factor of two (see Jackson et al., 2011b, 2020). The IPS analyses at 327 MHz only allow data from beyond 11.5°

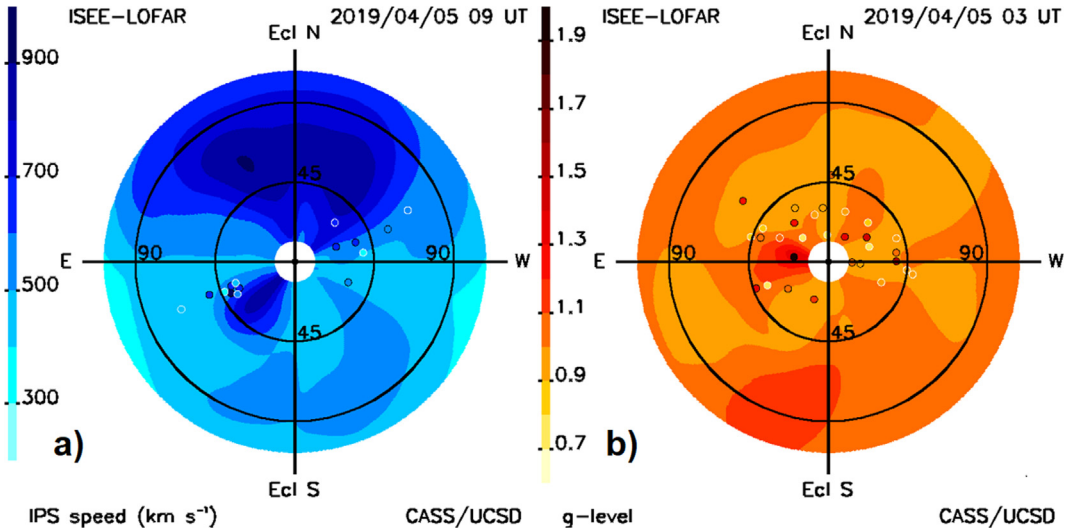

Fig. 11. The second PSP close pass near 21 UT April 4, 2019 shown as fisheye skymaps with sources used during the period superimposed. **a)** Modeled IPS perpendicular velocity values fit to the radio source LoS observed values from LOFAR. **b)** modeled and observed g-level source values from ISEE and LOFAR.

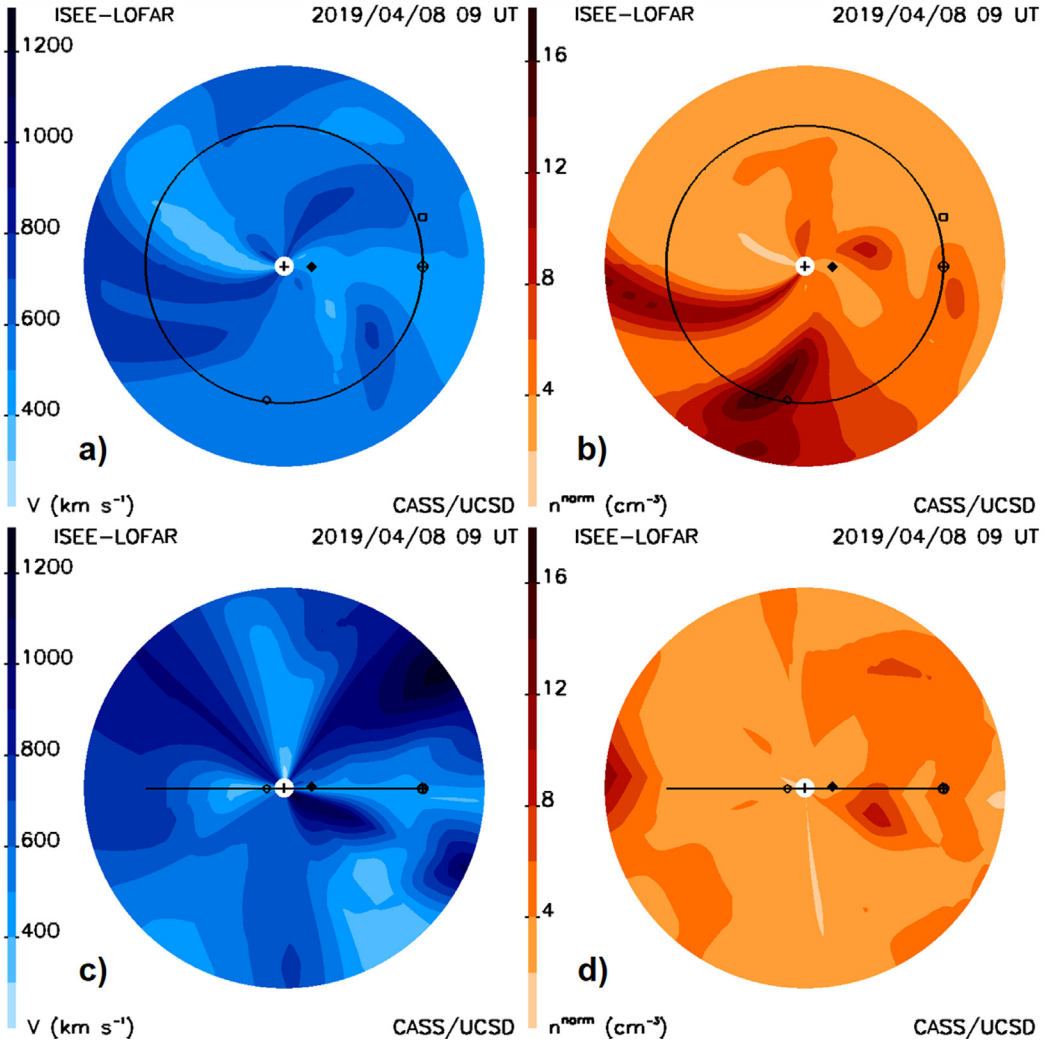

Fig. 12. **a) & b)** Cuts through the ecliptic plane of velocity and density at 09 UT on April 8, 2016. The ecliptic projections of locations STEREO A, PSP, and the BepiColombo spacecraft '□' are indicated on the plot. **c) & d)** Earth velocity and density ecliptic meridional cuts through Earth. The PSP spacecraft is on the Earth's meridian at a 0.20 AU solar distance at this time during the second close solar pass.

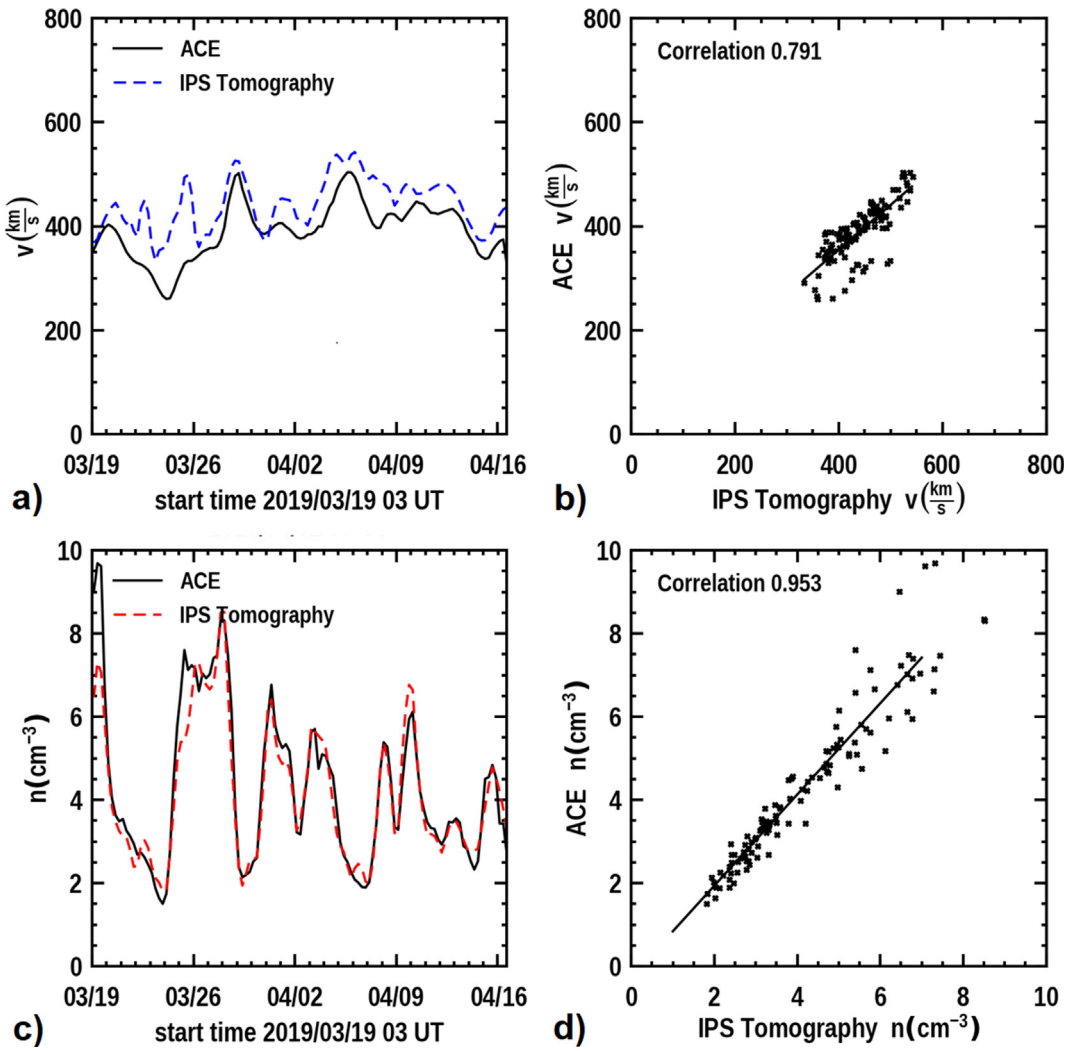

Fig. 13. **a)** IPS-derived velocities compared with measured ACE level zero in-situ velocities. **b)** A Pearson's "R" correlation shows an approximate one-two-one fit, and the correlation value of 0.79. **c)** & **d)** IPS-derived densities compared with measured ACE level zero in-situ densities have a correlation value of 0.95 and a one-to-one fit.

elongation (a P-Point distance of 0.19 AU) and the problem becomes more severe with LOFAR or Pushchino at 20° (0.34 AU) and 21° (0.36 AU), respectively. Although the limit of accurate correlation velocities can be determined closer to the Sun (see Kojima et al., 2013), than the weak scattering limit, the LoS weighting of Fig. 5 used to invert the tomography values will not be accurately determined there. Of necessity, we have needed to use only sources above the weak scattering limit to provide our tomographic analyses. Since the IPS analyses only fit solar wind observations using mass and mass flux conservation without considering solar wind acceleration or CME deceleration through this mechanism beyond this solar distance, this delay was assumed confined to the region below our lower observation limit: Thus, prior to this we have been unable to judge how well our analyses operates below or close to these distances.

For the first PSP solar pass on November 6, 2018 at 0.17 AU the original tomographic in-situ analyses from the IPS and PSP are shown for density in Fig. 16. At this time, outflowing material from an enhancement that is present at Earth also appears present to some extent at the PSP spacecraft in the 3-D reconstructed ecliptic plots. However, the in-situ measurements at PSP appear to substantiate slower outward-flowing solar wind speed by an enhancement of density in Fig. 16 over those of the tomography by at least a factor of two near the time of closest approach. We present these density analyses without normalization to distance to show that indeed the density becomes larger as the Parker distance to the Sun becomes closer in both in-situ measurement and in the 3-D reconstructions. The main density peak in both time series has approximately the same shape at the time of closest approach. Velocities, also reflect this acceleration difference by providing in-situ measurements that average ~200 kms^{-1}, and are lower than any of the in-situ measurements or 3-D reconstruction analyses presented near 1 AU by about a factor of almost two. These velocity and density results are consistent with

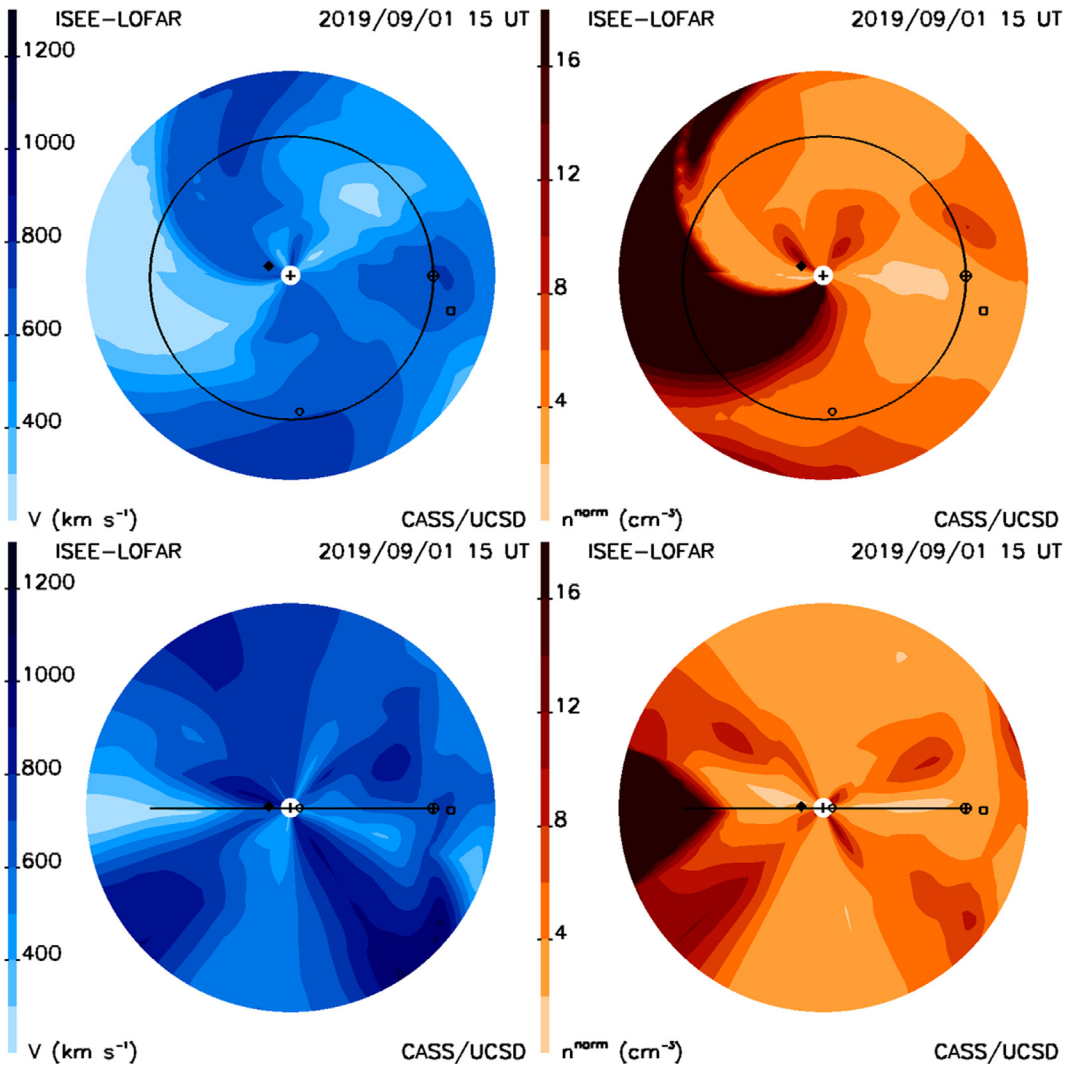

Fig. 14. **a) & b)** Cuts through the ecliptic plane of velocity and density at 15 UT on September 1, 2019. The ecliptic projections of locations STEREO A, PSP and the BepiColombo spacecraft '□' are indicated on the plot. **c) & d)** Earth velocity and density ecliptic meridional cuts through Earth. The PSP spacecraft is on the Earth's meridian at a 0.20 AU solar distance at this time during the second close solar pass.

the need to conserve mass flux on a global scale under the assumption of radial transport. To some extent this same general analysis inconsistency prevails for the second and third PSP solar passes we have studied where the close PSP passes provide higher in-situ densities than those 3-D reconstructed and lower in-situ velocities. However, to accurately depict this acceleration more precisely for different structures and the background solar wind will require more extensive study using a model of the presumed background solar wind acceleration, as well as better fits (or a revision) of Eq. (4), for these and further PSP close passes, and is beyond the scope of this current article.

5. Better results from WIPSS and the 3-D reconstructions

Clearly data from worldwide IPS stations helps provide more complete coverage both throughout the year and during nighttime hours when any one given station becomes blind to the fastest events traveling outward from the Sun. Continuous velocity coverage, especially using multi-site analyses, is difficult since each radio array needs to be maintained, and outages of large antennas are always present during the year from power interruptions, equipment and computer failures and weather related effects. There has been considerable effort to provide velocity measurements pioneered at the Ooty radio observatory (Manoharan and Anathathkrishnan, 1990) using single site analyses, and this has worked well in specific instances in the UCSD 3-D reconstructions to match in-situ data (Bisi et al., 2009). However this technique does not always work well, especially for weak radio sources see Chang et al. (2019) for a more complete assessment, where this type of analysis is compared with multi-site analysis. The advantage of this type of analysis is that it reduces the number of radio observatories required to provide a velocity measurement, and thus minimizes the inherent engineering

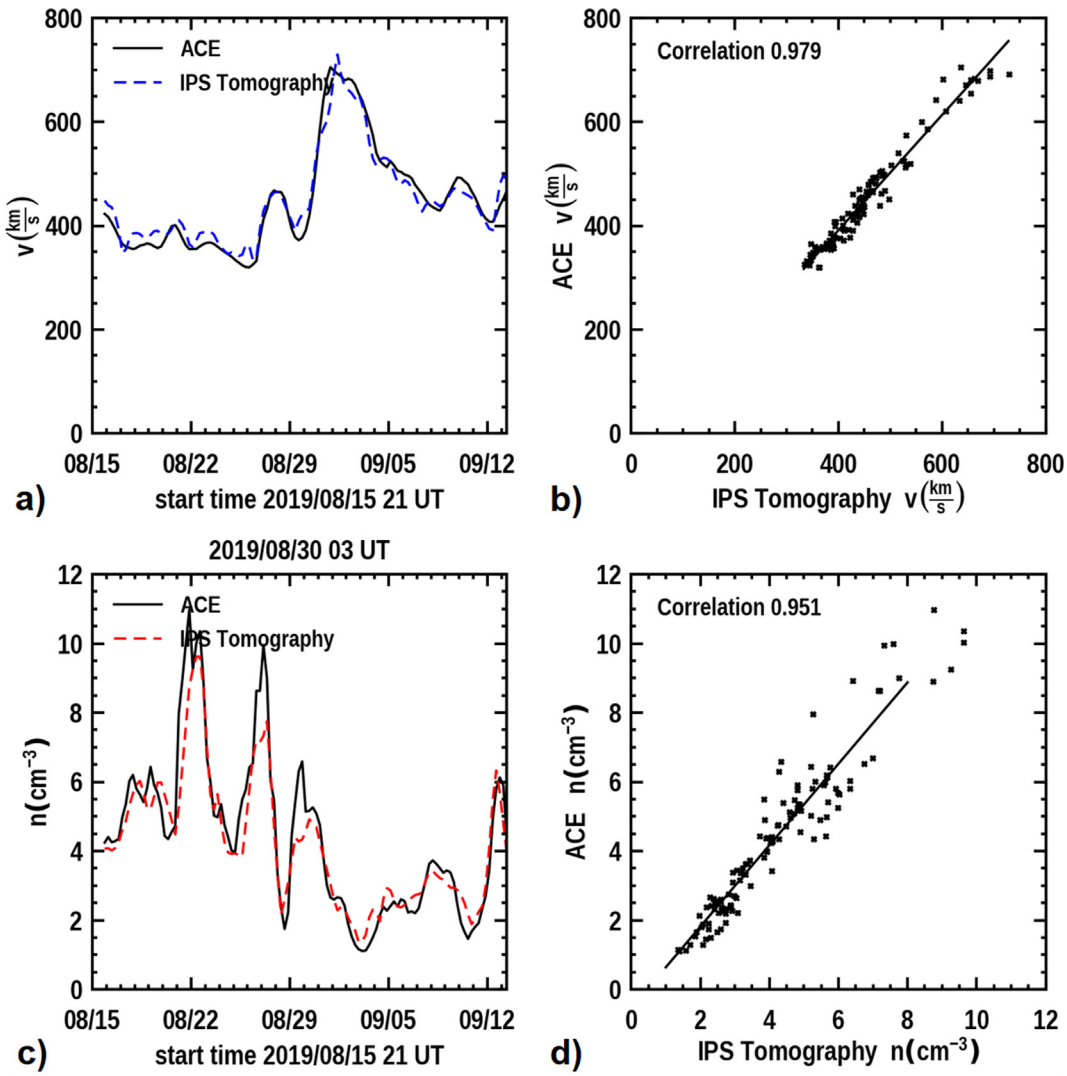

Fig. 15. **a)** IPS-derived velocities compared with measured ACE level zero in-situ velocities. **b)** A Pearson's "R" correlation shows an approximate one-two-one fit, and the correlation value of 0.79. **c)** & **d)** IPS-derived densities compared with measured ACE level zero in-situ densities have a correlation value of 0.95 and a one-to-one fit.

and land use problems associated with maintenance of more than one radio array near any given Earth longitude.

The discussion section indicates one way that the PSP solar passes can help provide a better analysis of the IPS globally than by fitting data to in-situ measurements at Earth. We have explored this to some extent at UCSD by using a power law falloff for density (and a subsequent increase in velocity to maintain a constant mass flux assuming radial expansion) as well as modifications to Eq. (4). This can provide better fit densities and velocities at both Earth and PSP, but does not work as well as it should, partly because we have not yet found a suitable method to provide an adequate representation of the background velocity increase close to the solar surface. These analyses will require confirmation from other LoS measurements, namely those from pulsar dispersion measures, where so far there has been little evidence that LoS measurements nearest the Sun provide higher densities than those determined by current IPS calibration techniques (Tiburzi et al., 2022).

Further advances in the 3-D reconstruction technique since the year 2004 have involved providing boundaries from the UCSD kinematic model to drive different 3-D MHD modeling efforts including the ENLIL model (Odstrcil et al., 2005, 2008; Jackson et al., 2015). Although ENLIL has been demonstrated to provide better-defined shock boundaries than the kinematic modeling, there are generally too few LoS from the IPS to provide better detail and timing from these observations so far. In addition even more recently ENLIL has been used as a kernel in the 3-D tomography (Jackson et al., 2020) with the refinement of these results still ongoing. The SUSANOO 3-D MHD modelling technique (Iwai et al., 2022) also uses IPS data from ISEE, Japan to help modify its CME inputs. This analysis uses ensemble runs to alter an assumed spheromak shape with many settable parameters that is directed into a

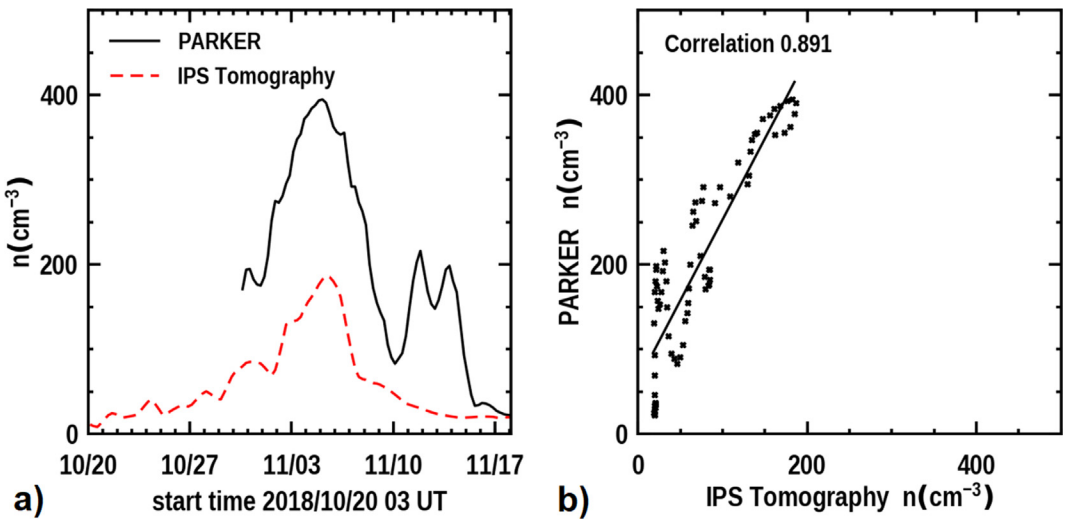

Fig. 16. **a)** IPS-derived densities compared with measured PSP in-situ velocities and densities over the Carrington interval during the PSP first close solar pass. **b)** Pearson's "R" correlation for the density are shown. The value of 0.89 partly reflects the large change in density as the spacecraft gets close to the Sun.

background solar wind model away from the Sun at the time of near solar surface indicators of the CME.

3-D MHD models provide more physics including the formation of shocks, non-radial transport, and solar wind acceleration upward from 0.1 AU through heating and solar wind expansion using the assumption that heliospheric plasma behaves as a fluid with a single polytrophic index. This shows an acceleration of the solar wind upwards from 0.1 AU, but is generally untested at PSP to Earth distances when PSP is near perihelion. The polytrophic index value is uncertain for numerous reasons and unknown effects including the possibility that the solar wind may be accelerated in part due to direct momentum addition through a system that does not involve temperature. Whether this acceleration is ubiquitous and assists in all manner of heliospheric structures, including CMEs that accelerate rapidly near the solar surface and then decelerate probably partly for reasons other than fast speeds catching up with slow (e.g., Lin and Chen, 2022), is still to be determined.

Finally, it is worth mentioning that the very highest-resolved kinematic model 3-D density reconstructions that have been accomplished with the orbiting Solar Mass Ejection Imager (SMEI - Jackson et al., 2004) analyses providing ~one-hour cadences near Earth (Jackson et al., 2020). These analyses with millions, rather than thousands of LoS available to the IPS show that at least some CMEs appear highly mottled and corrugated at one-degree spatial scales. This is an indication that previous modeling efforts have averaged over this corrugation and show only a smoothed version of CME structure (and presumably also background solar wind structure) at 1 AU as a remnant of variable velocities and densities, observed most recently as "switchbacks" in PSP in-situ measurements closer to the Sun (Bale et al., 2019). Although the present IPS analyses cannot hope to provide this many LoS in the near future to certify this result, the velocities at lower resolution provide the general background to shape the solar wind structures and provide a more exact background of solar wind speeds in which these structures are 3-D reconstructed at higher resolution.

6. Conclusions

Currently, the ISEE data set is the only one that provides a latency short-enough to enable 3-D forecasts and updates of plasma structures using the UCSD reconstruction analyses. Even so, the way to provide a better forecasting result is shown by these analyses, when different worldwide results are combined. When all stations work together even the fastest transient events can be forecast, and the results can be used to provide updates as these structures move outward from the Sun prior to their arrival at 1 AU. The long heritage and careful data-taking by the group at ISEE, Japan, have pioneered these techniques over many years, and this is explained here so that it can be followed by others to provide IPS results that can be fit without modification into the UCSD 3-D reconstruction technique. Beyond this, the UCSD kinematic and MHD analysis are continually being refined as more information and in-situ measurements from the inner heliospheric spacecraft monitors become available. In the next steps we expect to utilize these now-available in-situ results to provide even better fits globally throughout the inner heliosphere from the nearest distances of the Sun probed by PSP and as far outward to the planet Mars and beyond.

Declaration of Competing Interest

The authors declare that they have no known competing financial interests or personal relationships that could have appeared to influence the work reported in this paper.

Acknowledgements

The authors wish to thank P. Paul Hick for his many contributions to these studies, and his help to provide much of the original work on the IPS 3-D reconstruction programming and its display. B.V. Jackson, A. Buffington, L. Cota, and M. Bracamontes acknowledge funding from NASA contracts 80NSSC17K0684, 80NSSC21K0029, and AFOSR contract FA9550-19-1-0356 to the University of California, San Diego. The multi-station IPS observations at 327 MHz were conducted under the solar wind program of ISEE that have supported M. Tokumaru and K. Fujiki. This paper is based in part on data obtained with the International LOFAR Telescope (ILT) under project code LT10_001. LOFAR (van Haarlem et al., 2013) is the Low Frequency Array designed and constructed by ASTRON. It has observing, data processing, and data storage facilities in several countries, that are owned by various parties (each with their own funding sources), and that are collectively operated by the ILT foundation under a joint scientific policy. The ILT resources have benefitted from the following recent major funding sources: CNRS-INSU, Observatoire de Paris and Université d'Orléans, France; BMBF, MIWF-NRW, MPG, Germany; Science Foundation Ireland (SFI), Department of Business, Enterprise and Innovation (DBEI), Ireland; NWO, The Netherlands; The Science and Technology Facilities Council, UK; Ministry of Science and Higher Education, Poland. R. Fallows, M.M. Bisi, and D. Barnes were partially supported by the LOFAR4SW project, funded by the European Community's Horizon 2020 Programme H2020 INFRADEV-2017-1 under grant agreement 777442. O. Chang acknowledges support from the European Union's Horizon 2020 Research and Innovation Program under the Marie Sklodowska-Curie grant agreement 665593 awarded to the Science and Technology Facilities Council. I. Chashei, and S. Tyul'bashev acknowledge the BSA3 technical team for the IPS data and observations. All general format IPS data sets used in the analyses are available at: ftp://cass185.ucsd.edu/data/gen_ips.

Appendix A. *A.1. The IPS standard format*

In 2014 with UCSD, the Korean Space Weather Center, RAL Space, ISEE, and the then newly established Space Weather Service Mexico (SCiESMEX) hosted by the Universidad Nacional Autonoma de Mexico (UNAM) in Morelia, Mexico, began promoting a combined IPS effort to join all IPS instruments into a world group. With others including the Ooty, India IPS radio array, the Pushchino, Russia Big Scanning Array, the world IPS leaders began the concept of a Worldwide Interplanetary Scintillations Stations (WIPSS) network. At the Third Remote Sensing Workshop held 20–24 October 2015, held in Morelia, Michoacan, Mexico; 1) A standardized IPS format was settled upon; 2) All participants agreed to share their data and host the requisite websites for this sharing and displaying their data sets in near real time. Within a few months following the Morelia workshop, UCSD modified its tomography program to use a new standardized IPS format, and provide simultaneous inputs from six or more different radio observatories. Although much more informative data about each observation is generally available derived from the observations as explained in part in the introduction, the standard format settled upon lists each radio source observed at a given time on a single ASCII text line along with its derived plasma parameters. This ASCII row begins as: (Date MidObsUT Dur. Site Freq BW Source Size RA-J2000). The following next values are the same for a second-best data set from a given site or different-type analysis of the same source (i.e., single-sites values instead of CCF values), and are repeated as: Vel. V-err g-value g-err Method. A list of the parameters and their spaces taken in ASCII format is given in Table 1. Each of the values in Table 1 have a space after them, or indicate the following value is negative. The number in parenthesis at the end of each listed item gives the total number of spaces allotted to each entry including the preceding space, if present. The values used by the current UCSD tomography, are the Date, MidObsUT, Freq, Source, Size, RA-J2000, Dec-J2000, Vel, V-err, *g*-value, and *g*-err. Unknown values such as source sizes used to help provide LoS weights at a given frequency, are given values with minus nines (−999). In these cases the values are substituted for by the replacement of general number known for most sources at this frequency. For velocities where only two sites are used, an error cannot be determined, and these source values given −999 values can either be used (or not) in the 3-D reconstructions.

A.2. Article source selection

The IPS 3-D reconstructions can be used with sources selected with lowest errors, or tuned to provide best results

Table 1
List of Standard Format parameters.

Date – Date of the observation yyyymmdd	(8)
MidObsUT - Middle time in UT of the observation	(9)
Dur - Length of the observation in minutes	(5)
Site - Which observing system/site is used	(5)
Freq - The central observing frequency in MHz	(5)
BW - The bandwidth of the observation in MHz	(3)
Source - Source name (usually as 3C/4C/CTA/J2000)	(6)
Size - Angular source size in milli arc seconds	(8)
RA-J2000 - Right Ascension in J2000 coordinates	(10)
DC-J2000 - Declination in J2000 coordinates	(10)
Limb - East or West limb of the Sun	(4)
Dist. - Distance from the P-Point in solar radii	(9)
Lat. - Heliographic Latitude of the P-Point	(6)
PA - Position Angle from solar North (same as LASCO)	(7)
Elong. - Elongation angle from the Sun in degrees	(6)
Vel. - Best velocity value	(7)
V-err - Error in best velocity value	(7)
g-value - Best g-level value	(7)
g-err - Error in best g-level value	(7)
Method - Method used for the best values	(8)

Table 2
Source number distribution from each site and Carrington interval.

Period	Velocity source #'s			Velocity Total #'s	g-level source #'s			g-level Total #'s	in-situ V	in-situ N
	ISEE	LOFAR	BSA3		ISEE	LOFAR	BSA3			
2016	296	443	0	739	2809	172	989	3970	862 (CELIAS)	853 (CELIAS)
PSP Pass 1	345	443	–	788	2473	151	–	2624	1093 (ACE)	1078 (ACE)
PSP Pass 2	60	436	–	496	2362	153	–	2515	1254 (ACE)	1246 (ACE)
PSP Pass 3	293	690	–	983	2741	438	–	3179	1259 (ACE)	1245 (ACE)

from the different data sets from each source from any one site, or can use all values given when these are available. In the analysis presented for the depictions shown in this article, the source error was not considered in the 3-D reconstructions for source selection, and for ISEE data only the single-site g-level values from the Toyokawa array, and only three- or two-site velocity values from all arrays were used. The way to derive error values for different sources has not yet been certified among the different IPS groups, and has not yet been shown to provide meaningful comparisons between sites. These errors could allow different weights to be placed on each LoS, and if they were, could provide an analysis weighted to include best source values. Thus, these source restriction allotments and the analyses from them may change as more 3-D reconstruction analysis information or IPS data from different radio sites becomes available.

For each of the four 3-D reconstructions presented in this article, the data for them come from the different radio sites. Table 2. provides specific information about the numbers of radio sources and the numbers of hour averages of in-situ data used for the velocity and density 3-D reconstruction analyses over the Carrington rotation intervals from each site.

References

Baker, D.N., Li, X., Pulkkinen, A., Ngwira, C.M., Mays, M.L., Galvin, A.B., Simunac, K.D.C., 2013. A major solar eruptive event in July 2012: Defining extreme space weather scenarios. Space Weather 11 (10), 585–591. https://doi.org/10.1002/swe.20097.

Bale, S.D., Badman, S.T., Bonnell, J.W., Bowen, T.A., Burgess, D., Case, A.W., Cattell, C.A., Chandran, B.D.G., Chaston, C.C., Chen, C.H.K., Drake, J.F., Dudok de Wit, T., Eastwood, J.P., Ergun, R.E., Farrell, W.M., Fong, C., Goetz, K., Goldstein, M., Goodrich, K.A., Harvey, P.R., Hornbury, T.S., Howes, G.G., Kasper, J.C., Kellogg, P.J., Klimchuk, J.A., Korreck, K.E., Krasnoselskikh, V.V., Krucker, S., Laker, R., Larson, D.E., MacDowall, R.J., Maksimovic, M., Malaspina, D.M., Martinez-Oliveros, J., McComas, D.J., Meyer-Vernet, N., Moncuquet, M., Mozer, F.S., Phan, T.D., Pulupa, M., Raouafi, N.E., Salem, C., Stansby, D., Stevens, M., Szabo, A., Velli, M., Woolley, T., Wygant, J.R., 2019. Highly structured slow solar wind emerging from an equatorial coronal hole. Nature 576, 237–241. https://doi.org/10.1038/s41586-019-1818-7.

Bisi, M.M., Jackson, B.V., Clover, J.M., Manoharan, P.K., Tokumaru, M., Hick, P.P., Buffington, A., 2009. 3D reconstructions of the early-November 2004 CDAW geomagnetic storms: analysis of Ooty IPS speed and density data. Annales Geophysicae 27, 4479–4489.

Bisi, M.M., Fallows, R.A., Sobey, C., Eftekhari, T., Jensen, E.A., Jackson, B.V., Yu, H.-S., Hick, P.P., Odstrcil, D., Tokumaru, M., 2016. Worldwide Interplanetary Scintillation (IPS) and Heliospheric Faraday Rotation Plans and Progress. In: The IPSP South African National Space Agengy Space Weather Research Forum, Hermanus, South Africa, 20 January.

Bisi, M.M., Gonzalez-Esparza, J.A., Jackson, B., Aguilar-Rodriguez, E., Tokumaru, M., Chashei, I., Tyul'bashev, S., Manoharan, P., Fallows, R., Chang, O., Yu, H.-S., Fujiki, K., Shishov, V., Barnes, D., 2017. The Worldwide Interplanetary Scintillation (IPS) Stations (WIPSS) Network in support of Space-Weather Science and Forecasting. Paper presented at Geophysical Res. Abstracts, EGU General Assembly, Vienna, Austria, 23-28 April.

Breen, A.R., Moran, P.J., Varley, C.A., Wilkinson, W.P., Williams, P.J.S., Coles, W.A., Grall, R.R., Klinglesmith, M.T., Markkanen, J., 1997. EISCAT measurements of the solar wind: Observations of interaction regions. Phys. Chem. Earth 22 (5), 387–390. https://doi.org/10.1016/S0079-1946(97)00163-8.

Chang, O., Bisi, M.M., Aguilar-Rodriguez, E., Fallows, R.A., Gonzalez-Esparza, A., Chashei, I., Tyul'bashev, S., 2019. Single-Site IPS Power Spectra Analysis for Space Weather Products Using Cross-Correlation Function Results From EISCAT and MERLIN IPS Data. Space Weather 17, 1114–1130. https://doi.org/10.1029/2018SW002142.

Clarke, M.E., 1964. Two topics in radiophysics. I. Some observations of discrete radio sources. II. An investigation of ionospheric irregularities using a radio signal from an artificial satellite. University of Cambridge, Unpublished Ph.D. Thesis.

Cliver, E.W., Dietrich, W.F., 2013. The 1859 space weather event revisited: limits of extreme activity. J. Space Weather Space Clim. 3 (A3), (15 pages). https://doi.org/10.1051/swsc/2013053.

Domingo, V., Fleck, B., Poland, A.I., 1995. The SOHO mission: An overview. Sol. Phys. 162, 1–37.

Fallows, R.A., Bisi, M.M., Iwai, K., Jackson, B.V., Zhang, P., Zucca, P., 2022. Application of Novel Interplanetary Scintillation Visualizations using LOFAR: A Case Study of Merged CMEs from September 2017. Adv. Space Res. (this issue)

Gapper, G.R., Hewish, A., Purvis, A., Duffett-Smith, P.J., 1982. Observing interplanetary scintillation disturbances from the ground. Nature 296, 633–636.

Gonzalez-Esparza, J.A., De la Luz, V., Corona-Romero, P., Mejia-Ambriz, J.C., Gonzalez, L.X., Sergeeva, M.A., Romera-Hernandez, E., Aguilar-Rodriguez, E., 2017. Mexican Space Weather Service (SCiESMEX). Space Weather 15, 3–11. https://doi.org/10.1002/2016SW001496.

Hewish, A., Scott, P.F., Wills, D., 1964. Interplanetary scintillation of small diameter radio sources. Nature 203, 1214–1217.

Houminer, Z., 1971. Corotating plasma streams revealed by interplanetary scintillation. Nature Phys. Sci. 231, 165–167.

Hovestadt, D., Hilchenbach, M., Bürgi, A., Klecker, B., Laeverenz, P., Scholer, M., Grünwaldt, H., Axford, W.I., Livi, S., Marsch, E., Wilken, B., Winterhoff, H.P., Ipavich, F.M., Bedini, P., Coplan, M.A., Galvin, A.B., Gloeckler, G., Bochsler, P., Balsiger, H., Fischer, J., Geiss, J., Kallenbach, R., Wurz, P., Reiche, K.-U., Gliem, F., Judge, D.L., Ogawa, H.S., Hsieh, K.C., Möbius, E., Lee, M.A., Managadze, G.G., Verigin, M.I., Neugebauer, M., 1995. CELIAS - Charge, Element and Isotope Analysis System for SOHO. Sol. Phys. 162, 441–481. https://doi.org/10.1007/BF00733436.

Iwai, K., Fallows, R.A., Bisi, M.M., Shiota, D., Jackson, B.V., Tokumaru, M., Fujiki, K., 2022. Magnetohydrodynamic simulation

of coronal mass ejections using interplanetary scintillation data observed from multiple stations. Adv. Space Res., this issue

Jackson, B.V., Hick, P.L., Kojima, M., Yokobe, A., 1998. Heliospheric Tomography Using Interplanetary Scintillation Observations 1. Combined Nagoya and Cambridge data. J. Geophys. Res. 103, 12049–12067.

Jackson, B.V., Buffington, A., Hick, P.P., 2001. A heliospheric imager for Solar Orbiter. In: Proc. 'Solar Encounter: The First Solar Orbiter Workshop', May 14-18, 2001, Santa Cruz de Tenerife, Spain, ESA SP-493, pp. 251–254.

Jackson, B.V., Hick, P.P., Buffington, A., Kojima, M., Tokumaru, M., Fujiki, K., Ohmi, T., Yamashita, M., 2003. Time-dependent tomography of hemispheric features using interplanetary scintillation (IPS) remote-sensing observations. In: Velli, M., Bruno, R., Malara, F., (Eds.), Solar Wind Ten, AIP Conference Proceedings, vol. 679, pp. 75–78.

Jackson, B.V., Buffington, A., Hick, P.P., Altrock, R.C., Figueroa, S., Holladay, P.E., Johnston, J.C., Kahler, S.W., Mozer, J.B., Price, S., Radick, R.R., Sagalyn, R., Sinclair, D., Simnett, G.M., Eyles, C.J., Cooke, M.P., Tappin, S.J., Kuchar, T., Mizuno, D., Webb, D.F., Anderson, P.A., Keil, S.L., Gold, R.E., Waltham, N.R., 2004. The Solar Mass Ejection Imager (SMEI) Mission. Sol. Phys. 225, 177–207.

Jackson, B.V., Hick, P.P., Buffington, A., Bisi, M.M., Clover, J.M., Tokumaru, M., 2008a. Solar Mass Ejection Imager (SMEI) and Interplanetary Scintillation (IPS) 3D-Reconstructions of the Inner Heliosphere. Adv. Geosci. 21, 339–366.

Jackson, B.V., Bisi, M.M., Hick, P.P., Buffington, A., Clover, J.M., Sun, W., 2008b. Solar Mass Ejection Imager (SMEI) 3D reconstruction of the 27–28 May 2003 CME sequence. J. Geophys. Res. 113, A00A15. https://doi.org/10.1029/2008JA013224 (14 pages).

Jackson, B.V., Hick, P.P., Bisi, M.M., Clover, J.M., Buffington, A., 2010. Inclusion of in-situ Velocity Measurements in the UCSD Time-Dependent Tomography to Constrain and Better-Forecast Remote-Sensing Observations. Sol. Phys. 265, 245–256. https://doi.org/10.1007/s11207-010-9529-0.

Jackson, B.V., Hick, P.P., Buffington, A., Bisi, M.M., Clover, J.M., Tokumaru, M., Kojima, M., Fujiki, K., 2011a. Three-dimensional reconstruction of heliospheric structure using iterative tomography: A review. J. Atmospheric Sol.-Terrestrial Phys. 73, 1–9.

Jackson, B.V., Hamilton, M.S., Hick, P.P., Buffington, A., Bisi, M.M., Clover, J.M., Tokumaru, M., Fujiki, K., 2011b. SMEI 3-D reconstruction of density enhancements behind interplanetary shocks: in-situ comparison near Earth and at STEREO. J. Atmospheric Sol.-Terrestrial Phys. 73, 1317–1329. https://doi.org/10.1016/j.jastp.2010.11.023.

Jackson, B.V., Clover, J.M., Hick, P.P., Buffington, A., Bisi, M.M., Tokumaru, M., 2013. Inclusion of Real-Time in-situ Measurements into the UCSD Time-Dependent Tomography and Its Use as a Forecast Algorithm, to TI: Heliosphere - Observation & Modeling. Sol. Phys. 285, 151–165. https://doi.org/10.1007/s11207-012-0102-x.

Jackson, B.V., Odstrcil, D., Yu, H.-S., Hick, P.P., Buffington, A., Mejia-Ambriz, J.C., Kim, J., Hong, S., Kim, Y., Han, J., Tokumaru, M., 2015. The UCSD IPS Solar Wind Boundary and its use in the ENLIL 3D-MHD Prediction Model. Space Weather 13, 104–115. https://doi.org/10.1002/2014SW001130.

Jackson, B.V., Yu, H.-S., Buffington, A., Hick, P.P., Tokumaru, M., Fujiki, K., Kim, J., Yun, J., 2019. A daily determination of B_z using the Russell-McPherron effect to forecast geomagnetic activity. Space Weather 17, 639–652. https://doi.org/10.1029/2018SW002098.

Jackson, B.V., Buffington, A., Cota, L., Odstrcil, D., Bisi, M.M., Fallows, R.F., Tokumaru, M., 2020. Iterative Tomography: A Key to Providing Time-dependent 3-D Reconstructions of the Inner Heliosphere and the Unification of Space Weather Forecasting Techniques. Front. Astron. Space Sci. 7, 568429. https://doi.org/10.3389/fspas.2020.568429 (19 pages).

Kojima, M., Tokumaru, M., Watanabe, H., Yokobe, A., Asai, K., Jackson, B.V., Hick, P.L., 1998. Heliospheric Tomography Using Interplanetary Scintillation Observations 2. Latitude and Heliocentric Distance Dependence of Solar Wind Structure at 0.1-1 AU. J. Geophys. Res. 103, 1981–1989.

Kojima, M., Coles, W.A., Tokumaru, M., Fujiki, K., 2013. Scintillation Measurements of the Solar Wind Velocity in Strong Scattering Near the Sun. Sol. Phys. 283 (2), 519–540. https://doi.org/10.1007/s11207-012-0207-2.

Lin, C.-H., Chen, J., 2022. Drag Force on Coronal Mass Ejections (CMEs). J. Geophys. Res. https://doi.org/10.1029/2020JA028744.

Manoharan, P.K., 2010. Ooty interplanetary scintillation–Remote-sensing observations and analysis of coronal mass ejections in the heliosphere. Sol. Phys. 265, 137–157.

Manoharan, P.K., Anathathkrishnan, S., 1990. Determination of solar-wind velocities using single-station measurements of interplanetary scintillation. MNRAS 244, 691–695.

McComas, D.J., Bame, S.J., Barker, P., Feldman, W.C., Phillips, J.L., Riley, P., Griffee, J.W., 1998. Solar Wind Electron Proton Alpha Monitor (SWEPAM) for the Advanced Composition Explorer. Space Science Revs. 86, 563–612.

Odstrcil, D., Pizzo, V.J., Arge, C.N., Jackson, B.V., Hick, P.P., 2005. First Results from the 3-D MHD Heliospheric Simulations Driven by the SMEI/IPS Observations. In: *Proc. SPIE* **5901**, 31 July - 4 August San Diego, CA USA (presentation only).

Odstrcil, D., Pizzo, V.J., Arge, C.N., Bisi, M.M., Hick, P.P., Jackson, B. V., Ledvina, S.A., Luhmann, J.G., Linker, J.A., Mikic, Z., Riley, P., 2008. Numerical Simulations of Solar Wind Disturbances by Coupled Models. ASP Conf. Series Proc. 385, 167–173.

Ogilvie, K.W., Desch, M.D., 1997. The Wind spacecraft and its early scientific results. Adv. Space Res. 20 (445), 559–568.

Russell, C.T., Mewaldt, R.A., Luhmann, G.J., Mason, G.M., von Rosenvinge, T.T., Cohen, C.M.S., Leske, R.A., Gomez-Herrero, R., Klassen, A., Galvin, A.B., Simunac, K.D.C., 2013. The very unusual interplanetary coronal mass ejection of 2012 July 23: A blast wave mediated by solar energetic particles. Astrophys. J. 770, 38. https://doi.org/10.1088/0004-637X/770/1/38.

Stone, E.C., Frandsen, A.M., Mewaldt, R.A., Christian, E.R., Margolies, D., Ormes, J.F., Snow, F., 1998. The Advanced Composition Explorer, *Space Sci.* Rev. 86, 1–22.

Tokumaru, M., Kojima, M., Fujiki, K., Yokobe, A., 2000. Three-dimensional propagation of interplanetary disturbances detected with radio scintillation measurements at 327 MHz. J. Geophys. Res. 105 (A5), 10435–10454. https://doi.org/10.1029/2000JA900001.

Tokumaru, M., Kojima M., Fujiki, K., Yamashita, M., 2003. Global Structure of Interplanetary Coronal Mass Ejections Retrieved from the Model Fitting Analysis of Radio Scintillation Observations. In: Velli, M., Bruno, R., Malara, F. (Eds.), Solar Wind Ten, AIP Conference Proceedings, vol. 679, pp. 729–732.

Tokumaru, M., Kojima, M., Fujiki, K., Yamashita, M., Jackson, B.V., 2007. The source and propagation of the interplanetary disturbance associated with the full-halo coronal mass ejection on 2003 October 28. J. Geophys. Res. 112, A05106. https://doi.org/10.1029/2006JA012043 (7 pages).

Tokumaru, M., Kojima, M., Fujiki, K., Maruyama, K., Maruyama, Y., Ito, H., Iju, T., 2011. A newly developed UHF radio telescope for interplanetary scintillation observations: Solar Wind Imaging Facility. Radio Sci. 46, RS0F02. https://doi.org/10.1029/2011RS004694 (9 pages).

Tokumaru, M., Fujiki, K., Iwai, K., Tyul'bashev, S., Chashei, I., 2019. Coordinated Interplanetary Scintillation Observations in Japan and Russia for Coronal Mass Ejection Events in Early September 2017. Sol. Phys. 294, 87. https://doi.org/10.1007/s11207-019-1487-6 (15 pages).

Tiburzi, C., Jackson, B.V., Cota, L., Shaifullah, G.M., Fallows, R.A., Tokumaru, M., Zucca, P., 2022. Validation of Interplanetary scintillation –based tomography of heliospheric conditions using pulsar dispersion measures. Adv. Space Res. https://doi.org/10.1016/j.asr.2022.04.070 (in press, this issue).

van Haarlem, M.P., Wise, M.W., Gunst, A.W., Heald, G., McKean, J.P., Hessels, J.W.T., de Bruyn, A.G., Nijboer, R., Swinbank, J., Fallows,

R., Brentjens, M., Nelles, A., Beck, R., Falcke, H., Fender, R., Hörandel, J., Koopmans, L.V.E., Mann, G., Miley, G., Röttgering, H., Stappers, B.W., Wijers, R.A.M.J., Zaroubi, S., van den Akker, M., Alexov, A., Anderson, J., Anderson, K., van Ardenne, A., Arts, M., Asgekar, A., Avruch, I.M., Batejat, F., Bähren, L., Bell, M.E., Bell, M. R., van Bemmel, I., Bennema, P., Bentum, M.J., Bernardi, G., Best, P., Ĥırzan, L., Bonafede, A., Boonstra, A.-J., Braun, R., Bregman, J., Breitling F., van de Brink R. H., Broderick J., Broekema P. C., Brouw W. N., Brüggen M., Butcher H. R., van Cappellen W., Ciardi, B., Coenen, T., Conway, J., Coolen, A., Corstanje, A., Damstra, S., Davies, O., Deller, A.T., Dettmar, R.-J., van Diepen, G., Dijkstra, K., Donker, P., Doorduin, A., Dromer, J., Drost, M., van Duin, A., Eislöffel, J., van Enst, J., Ferrari, C., Frieswijk, W., Gankema, H., Garrett M. A. de Gasperin, F., Gerbers M., de Geus, E., Grießmeier, J.-M.,Grit, T., Gruppen, P., Hamaker, J. P., Hassall, T., Hoeft, M., Holties, H. A., Horneffer, A., van der Horst, A., van Houwelingen, A., Huijgen, A., Iacobelli, M., Intema, H., Jackson, N., Jelic, V., de Jong, A., Juette, E., Kant, D., Karastergiou, A., Koers, A., Kollen, H., et al., 2013. LOFAR: The LOw-Frequency Array. *Astron. Astrophys.*. **556**, A2., (53 pages), https://doi.org/10.1051/0004-6361/201220873.

Viall, N.M., DeForest, C.E., Kepko, L., 2021. Mesoscle Structures in the Solar Wind. Front. Astron. Space Sci. 7, 735034. https://doi.org/10.3389/fspas.2021.735034 (18 pages).

Young, A.T., 1971. Interpretation and interplanetary scintillation. Astrophys. J. 168, 543–562.